HHS Public Access

Author manuscript

Nature. Author manuscript; available in PMC 2019 October 17.

Published in final edited form as:

Nature. 2019 May ; 569(7754): 73–78. doi:10.1038/s41586-019-1118-2.

Fatty acid transporter 2 reprograms neutrophils in cancer

Filippo Veglia[1], **Vladimir A. Tyurin**[2], **Maria Blasi**[3], **Alessandra De Leo**[4], **Andrew Kossenkov**[1], **Laxminarasimha Donthireddy**[1], **To Tsun Ki Jerrick**[5], **Zach Schug**[6], **Subhasree Basu**[6], **Fang Wang**[1], **Emanuela Ricciotti**[5], **Concetta DiRusso**[7], **Maureen E. Murphy**[6], **Robert H. Vonderheide**[5], **Paul M. Lieberman**[4], **Charles Mulligan**[8], **Brian Nam**[8], **Neil Hockstein**[8], **Gregory Masters**[5,8], **Michael Guarino**[8], **Cindy Lin**[1], **Yulia Nefedova**[1], **Paul Black**[7], **Valerian E. Kagan**[2,9], and **Dmitry Gabrilovich**[1,10]

[1]–Immunology, Microenvironment and Metastasis Program, The Wistar Institute, Philadelphia, PA, 19104;

[2]–Department of Environmental and Occupational Health, University of Pittsburgh, PA, 15219;

[3]–Duke Human Vaccine Institute, Duke University School of Medicine, Durham, NC, 27710;

[4]–Gene Expression and Regulation Program, The Wistar Institute, Philadelphia, PA, 19104;

[5]–University of Pennsylvania School of Medicine, Philadelphia, PA, 19104,

[6]–Program in Molecular and Cellular Oncogenesis, The Wistar Institute, Philadelphia, PA, 19104

[7]–Department of Biochemistry, University of Nebraska, Lincoln, NE 68588

[8]–Helen F Graham Cancer Center at Christiana Care Health System, Wilmington, DE,

[9]–Departments of Chemistry, Pharmacology and Chemical Biology, Radiation Oncology, University of Pittsburgh, USA, Laboratory of Navigational Redox Lipidomics, IM Sechenov Moscow State Medical University, Russia

Summary

[10]–Address for correspondence: The Wistar Institute, 3601 Spruce Str. Philadelphia, PA, 19104, dgabrilovich@wistar.org.

Authors Contributions

F.V. – participated in research design, performed most of the experiments, wrote manuscript, V.A.T. – performed lipidomics experiments, M.B. – prepared lentiviruses for experiments, A.D.L. – performed ChIP assay; L.D. – performed animal treatment experiments; A.K. – performed the analysis of RNAseq data; T.K.J. – performed some immunological experiments; Z.S. – performed metabolomics experiments, wrote manuscript, S.B. – performed seahorse experiments, F.W. – performed immunohistochemistry experiments; E.R. – generated COX2 KO cells; C.D. – generated lipofermata and wrote manuscript, M.E.M. – supervised metabolic experiments, reviewed manuscript, R.H.V. – supervised experiments with KPC mice, review manuscript, P.M.L. – supervised ChIP experiments, reviewed manuscript, C.M., B.N., N.H., G.M., M.G. – provided clinical samples; C.L. – generated mice with PMN targeted STAT5 deletion and performed *in vivo* experiments; Y.N. – generated mice with PMN targeted STAT5 deletion, reviewed manuscript, P.B. – produced lipofermata, reviewed manuscript, V. E. K. – obtained financial support for the study, designed experiments, supervised lipidomics analysis, wrote manuscript; D.I.G. – obtained financial support for the study, designed overall concept and specific experiments, supervised experiments, wrote manuscript.

Data availability statement. The data that support the findings of this study are available from the corresponding author upon reasonable request. Source data for each figure are provided in supplement. RNAseq data are deposited to GEO data repository, accession number GSE126885

Authors state no competing financial interests

Polymorphonuclear myeloid derived suppressor cells (PMN-MDSC) are pathologically activated neutrophils that are critically important for the regulation of immune responses in cancer. They contribute to the failure of cancer therapies and are associated with poor clinical outcomes. Despite the recent advances in understanding of the PMN-MDSC biology, the mechanisms responsible for pathological activation of neutrophils are not well defined, which limits selective targeting of these cells. Here, we report that mouse and human PMN-MDSC exclusively up-regulate fatty acid transporter protein 2 (FATP2). Over-expression of FATP2 in PMN-MDSC was controlled by GM-CSF, through the activation of STAT5 transcription factor. Deletion of FATP2 abrogated the suppressive activity of PMN-MDSC. The main mechanism of FATP2 mediated suppressive activity involved uptake of arachidonic acid (AA) and synthesis of prostaglandin E2 (PGE2). The selective pharmacological inhibition of FATP2 abrogated the activity of PMN-MDSC and substantially delayed tumor progression. In combination with check-point inhibitors it blocked tumor progression in mice. Thus, FATP2 mediates acquisition of immune suppressive activity by PMN-MDSC and represents a new target to selectively inhibit the functions of PMN-MDSC and improve the effect of cancer therapy.

Polymorphonuclear myeloid derived suppressor cells (PMN-MDSC) are pathologically activated neutrophils that accumulate in many diseases. These cells are critically important for the regulation of immune responses in cancer, promotion of tumor progression, and metastases, and their presence correlates with poor prognosis and negative response to immunotherapy[1–4]. Despite the fact that neutrophils and PMN-MDSC share same origin and the same differentiation pathways, PMN-MDSC have distinct genomic and biochemical features and are immunosuppressive[2]. The mechanisms responsible for pathological activation of neutrophils are not well defined, which limits selective targeting of these cells. We asked whether changes in lipid metabolism could contribute to pathological activation of PMN-MDSC. An accumulation of lipids in cancer has been shown in macrophages[5–7], dendritic cells (DC)[8–11], and total population of MDSC where it was associated with suppressive activity[12]. Here, we report a specific role of the fatty acid (FA) transport protein 2 (FATP2) in regulation of PMN-MDSC function.

FATP2 is selectively overexpressed by PMN-MDSC and controls their suppressive activity

We evaluated total lipid levels in $CD11b^{+}Ly6C^{lo}Ly6G^{+}$PMN-MDSC from spleens of tumor-bearing (TB) mice and neutrophils (PMN) with the same phenotype from spleens of tumor-free mice in transplantable models of EL-4 lymphoma, LLC lung carcinoma, and CT26 colon carcinoma as well as genetically engineered model (GEM) of pancreatic cancer (KPC). PMN-MDSC in all tested models showed substantially higher amounts of lipids than control PMN (Extended data Fig. 1a). Tumor explant supernatant (TES) promoted accumulation of lipids in PMN differentiated *in vitro* from bone marrow (BM) hematopoietic progenitor cells (HPC) (Extended data Fig. 1b). LC/MS lipidomics analysis of triglycerides (TG), the major component of lipid droplets[13] revealed that PMN-MDSC from spleen of TB mice had significantly more TG, than PMN from control mice (Extended data Fig. 1c). This effect was particularly robust (~8-fold) in TG containing arachidonic acid (AA). A similar analysis was performed in $CD11b^{+}Ly6C^{hi}Ly6G^{-}$ M-MDSC from TB mice

and monocytes with the same phenotype from tumor-free mice. In all tested models, M-MDSC had markedly increased lipid accumulation (Extended data Fig 1d).

Previous studies demonstrated that lipid accumulation in DCs was mediated by up-regulation of scavenger receptor CD204[8–10]. However, whereas the accumulation of lipids was abrogated in CD204 deficient (*Msr1*$^{-/-}$) DCs, it was not affected in PMN (Extended data Fig. 1e). These results were confirmed *in vivo* using BM chimeras of *Msr1*$^{-/-}$ and wild-type (WT) mice. Lack of CD204 did not abrogate lipid uptake by PMN-MDSC (Extended data Fig. 1f) and did not cancel their suppressive activity (Extended data Fig. 1g). Several membrane proteins have been implicated in trafficking of lipids, including CD206, CD36, FA binding proteins and FA transport proteins (FATP). The FATP family includes six members (FATP1–6), also known as solute carrier 27 (SLC27). FATP acts as long-chain FA transporter and an acyl-CoA synthetase (ACS)[14–16]. ACS converts free long-chain FA into fatty acyl-CoA esters, which can be used in many metabolic processes, including FA synthesis, oxidation, and complex lipid synthesis. We compared the expression of genes potentially involved in lipid uptake between PMN-MDSC from EL4 TB mice and control PMN using the gene expression array described previously[17]. PMN-MDSC had a much higher expression of *slc27a2*, which encodes FATP2. This was confirmed by qPCR (Fig. 1a). No up-regulation of other transporters and receptors involved in lipid accumulation was detected (Extended data Fig. 1h). In contrast to PMN-MDSC, M-MDSC showed a barely detectable expression of *slc27a2* in the same TB mice (Fig. 1b). DCs, spleen and tumor associated macrophages (TAM) had undetectable and CD8$^+$ T cells very low expression of *slc27a2* (Fig. 1c). Increased amount of FATP2 protein was confirmed by Western blot in PMN-MDSC isolated from spleens of TB mice (Extended data Fig. 2a) or generated *in vitro* with TES (Extended data Fig. 2b).

Next, we asked whether FATP2 might regulate the functionality of PMN-MDSC. To this end, we analyzed the function of PMN-MDSC isolated from *slc27a2*$^{-/-}$ mice. These mice were originally generated on SV129 background. Therefore, we established a syngeneic sarcoma (F244) in *slc27a2*$^{-/-}$ and WT mice. Tumors were spontaneously rejected in FATP2 KO mice (Extended data Fig. 2c). *Slc27a2*$^{-/-}$ mice were then backcrossed for 10 generations to C57BL/6 background. We found that in these mice, the growth of LLC and EL4 tumors was markedly slower than in WT mice (Fig. 1d). To test whether that effect was mediated by hematopoietic cells, we established BM chimeras by reconstituting lethally irradiated recipient congenic mice with WT or FATP2 KO BM cells. Tumors established in mice reconstituted with FATP2 KO BM cells grew substantially slower than did tumors in mice reconstituted with WT BM cells (Fig. 1e). Depletion of CD8$^+$ T cells LLC or EL4 TB mice completely abrogated the antitumor activity observed in FATP2 KO mice (Fig. 1f). To confirm a specific role of FATP2 depletion in PMN in the observed antitumor effect, we generated *slc27a2*$^{fl/fl}$ mice and crossed them with S100A8-cre mice to target the deletion to PMN (Extended data Fig. 2d). In the absence of FATP2 in PMN, the tumor grew markedly slower than in control mice (Fig. 1g). Loss of FATP2 did not affect the functionality of CD8$^+$ T cells (Extended data Fig. 2e).

Since the functionality of PMN-MDSC depends on tumor burden, we compared PMN-MDSC from WT and FATP2 KO TB mice depleted of CD8 T cells, which allow for the

analysis of mice with the same tumor size. In both, spleens and tumors of FATP2 KO mice, PMN-MDSC lost the ability to suppress antigen-specific $CD8^+$ T cell responses (Fig. 1h). In contrast, the suppressive activity of M-MDSC (Extended data Fig. 2f) or TAM (Extended data Fig. 2g) was not affected.

Expression of *slc27a4*, which encodes FATP4 was slightly up-regulated in PMN-MDSC (Extended data Fig. 1i). However, in contrast to FATP2 KO mice, no difference in tumor growth and suppressive function of PMN-MDSC were found between WT and FATP4 KO TB mice (Extended data Fig. 2h,i). CD36 has been shown to affect the lipid accumulation in different myeloid cells. Since tumors in CD36 KO mice may grow slower than in WT mice and growth depends on CD8 T cells[12], we analyzed the lipid levels in PMN-MDSC from CD36 KO and WT mice with CD8 T cell depletion. We found no difference in lipid accumulation in KO and WT PMN-MDSC (Extended data Fig. 2j,k).

Whole genome RNAseq was performed on spleen PMN-MDSC isolated from WT and FATP2 KO TB mice. Deletion of FATP2 resulted in significant changes in 1119 genes (FRD<5%, at least 2-fold) with 37 genes showing dramatic changes of at least 5-fold (Extended data Fig. 3a). There was an overall predominance of genes downregulated in FATP2 KO (Extended data Fig. 3b). Enrichment analysis of significantly affected genes using Ingenuity Pathway Analysis revealed that PMN-MDSC from FATP2 KO mice had a marked decrease of pro-inflammatory genes (Extended data Fig. 3c).

FATP2 regulates uptake of arachidonic acid and PGE2 synthesis by PMN-MDSC

We then investigated the role of FATP2 in regulating lipid accumulation by PMN-MDSC. Experiments were performed with PMN-MDSC isolated from WT and FATP2 KO LLC TB mice with depleted $CD8^+$ T cells. LC-MS analysis revealed a lower the total amounts of TG in FATP2 KO spleen PMN-MDSC than in WT PMN-MDSC and especially TG containing C20:4 AA (Fig. 2a). Polyunsaturated FA (PUFA), AA, C18:2 linoleic acid (LA), C22:5 eicosapentaenoic and C22:6 docosahexaenoic (DHA) FA were markedly reduced (Fig. 2b, Extended data 4a). No differences in the total content of cholesterol esters (CE) or arachidonoyl-containing CE were found (Extended data 4b). The presence of free AA and LA was decreased (Extended data 4c). The total content of phospholipids (PL) was not changed (Extended data Fig. 4d), whereas many molecular species of arachidonoyl-containing PL were markedly reduced (Fig. 2c, Extended data Fig. 4e). Thus, genetic elimination of FATP2 caused selective depletion of AA-containing species of PL. These finding are consistent with the previous observation that although FATP2 is not a selective transporter for AA, its overexpression favors increased uptake and trafficking of AA[16].

We next employed a method of stable isotope labeling using deuterated AA, (AAd11) and high mass accuracy/high resolution LC-MS with MS/MS fragmentation analysis to directly trace uptake of exogenously added AAd11 by PMN-MDSC from WT and FATP2 KO LLC TB mice. We detected significantly lower amounts of AAd11, as well as labeled PGE2d11 in FATP2 KO PMN-MDSC compared to WT PMN-MDSC (Fig. 2d). We also observed significant reduction of AAd11-containing PL (Fig. 2e, Extended Table 1). This was

consistent with the markedly reduced amounts of the total (unlabeled) free AA and its metabolite PGE2 (Extended data Fig. 4b), as well as unlabeled AA-containing PL (Extended data Fig. 4d). No significant differences were observed in the total amounts of palmitic acid (16:0), oleic acid (18:1), LA (18:2), alpha-linolenic acid (18:3), docosapentaenoic acid (22:5), and DHA (22:6) (Extended data Fig. 4 b).

Next, we asked whether lack of FATP2 affected metabolic activity of PMN-MDSC. Spleen PMN-MDSC deficient in FATP2 did not show changes in OXPHOS (Extended data Fig. 5a) and glycolysis (Extended data Fig. 5b) compared to WT PMN-MDSC. We studied FA oxidation (FAO) in more detail using incorporation of $^{13}C_{16}$-palmitate to TCA. No differences in labeled metabolites were found between WT and FATP2 KO PMN-MDSC (Extended data Fig. 5c). Neither splenic nor tumor PMN-MDSC from FATP2 KO mice showed changes in the expression of *cpt1a, hadha, or acadm*, major enzymes involved in FAO (Extended data Fig. 5d). There were also no differences in the uptake of the major nutrients between WT and FATP2 KO PMN-MDSC (Extended data Fig. 6). Taken together, these data indicate that lack of FATP2 does not affect FAO in PMN-MDSC.

AA is a key precursor of PGE2, which was implicated in the suppressive activity of MDSC in cancer[18–21] and PMN-MDSC from neonates[22]. We therefore sought to investigate whether FATP2 regulates the suppressive functions of PMN-MDSC through the accumulation of AA and the subsequent production and release of PGE2. Using LC/MS (Extended data Fig. 7a) and ELISA (Extended data Fig. 7b) we confirmed that PMN-MDSC produced and released significantly higher amount of PGE2 than control PMN. This was associated with higher expression of *ptges*, prostaglandin E synthase, a key enzyme in the synthesis of PGE2 (Extended data Fig. 7c). PMN-MDSC from FATP2 KO TB mice release significantly less PGE2 than WT PMN-MDSC (Fig. 2f). This was consistent with significantly lower amount of intracellular PGE2 in FATP2 deficient PMN-MDSC than in WT cells (Extended data Fig. 7b). Consistent with a reduced amount of substrate the expression of genes involved in PGE2 synthesis, *ptgs2* and *ptges*, were lower in FATP2 KO PMN-MDSC than in WT PMN-MDSC (Extended data Fig. 7d). No difference was found between WT and KO PMN-MDSC in the expression of genes commonly associated with MDSC activity, *arg1*, *nos2* (Extended data Fig. 7e). We transduced HPC with *scl27a2-gfp* or control lentivirus and differentiated to PMN in the presence of GM-CSF. Overexpression of *slc27a2* (Fig. 2g) resulted in increased production of PGE2 in GFP^+ PMN as compared to GFP^- PMN (Fig. 2h).

To test whether AA could drive the accumulation of suppressive PMN, we generated PMN from HPC in the presence of GM-CSF and AA and found that addition of AA favored the expansion of PMN-MDSC (Extended data Fig. 7f) that suppressed antigen specific T cell responses (Fig.2i). This suppressive activity was associated with a higher production of PGE2 (Fig.2j), increased expression of *nox2*, but not *arg1* or *nos2* (Extended data Fig. 7g). To verify the specific role of PGE2 in AA inducible suppressive activity of neutrophils, we generated PMN from COX2 deficient (*ptgs2*$^{-/-}$) HPC. In the absence of COX2 PGE2 synthesis was decreased (Fig. 2k). The presence of AA during PMN differentiation from *ptgs2*$^{-/-}$ HPC was not able to generate suppressive PMN-MDSC (Fig. 2l). Together, these

data suggested that FATP2 controls suppressive activity of PMN-MDSC via increased uptake of AA and synthesis of PGE2.

Slc27a2 promoter has a binding site for the transcription factor STAT5 (http://jaspar.genereg.net). STAT5 can be activated by GM-CSF, which plays a critical role in myelopoiesis and expansion of MDSC[23]. To explore whether GM-CSF might control *slc27a2* expression through STAT5 activation we treated PMN isolated from BM of tumor free mice with GM-CSF for 2 hrs. As expected, it caused a dose-dependent activation of STAT5 (pSTAT5) (Extended data Fig. 7h). This activation was associated with up-regulation of FATP2 (Fig. 3a). Chromatin immune precipitation (ChIP) demonstrated that STAT5 could directly bind to the *slc27a2* promoter (Fig. 3b). Conversely, GM-CSF failed to increase the expression of FATP2 in Stat5 deficient PMN (Fig. 3c). To confirm the role of STAT5 in controlling the expression of *slc27a2* in PMN, we crossed $Stat5^{fl/fl}$ mice with S100A8-cre mice to target the deletion of Stat5 to PMN. In the absence of Stat5 in PMN, the tumor growth was slower than in control mice (Extended data Fig. 7i). This was associated with lower expression of *slc27a2* in PMN (Extended data Fig. 7j). These data indicate that GM-CSF regulates the expression of *slc27a2* through the activation of pSTAT5.

Lipid accumulation and FATP2 expression in human PMN-MDSC

PMN-MDSC isolated from the blood of patients with head and neck, lung, or breast cancers accumulated more lipids than PMN from healthy donors (Fig. 3d). PMN-MDSC in tumors had higher amounts of lipids than PMN-MDSC in blood from the same patients (Fig. 3e). PMN-MDSC from cancer patients had higher expression of *SLC27A2* (Fig. 3f) and FATP2 (Fig. 3g) than control PMN. M-MDSC isolated from blood of cancer patients also had more lipids than monocytes from healthy donors (Extended data Fig.8a). However, there was no difference in the accumulation of lipids in M-MDSC isolated from blood and tumor of the same patient (Extended data Fig.8b). Recently, we identified LOX-1 as a marker of human PMN-MDSC[24]. Analysis of a gene expression array[24] revealed that $LOX1^{+}$ PMN-MDSC had higher expression of *SLC27A2*, but not other transporters as compared with $LOX\text{-}1^{-}$ PMN from the same patients (Extended data Fig.8c). The higher expression of *SLC27A2* in $LOX\text{-}1^{+}$ PMN-MDSC was validated by RT-qPCR (Fig. 3h). *SLC27A2* expression was associated with higher expression of *PTGES* (Extended data Fig.8d). In contrast, M-MDSC had lower expression of *SLC27A2* than monocytes (Extended data Fig.8e). Similar to the results obtained in mice, GM-CSF up-regulated pSTAT5 (Extended data Fig.8f), and FATP2 (Extended data Fig.8g).

Using LS/MS lipidomics we identified a substantially higher amount of total TG (Fig. 3i), and free AA, LA, and DHA (Fig. 3j) in PMN-MDSC from cancer patients than in PMN from healthy individuals. Higher amounts of PGE2 were detected in PMN-MDSC than in control PMN (Fig. 3k). The contents of total PE and arachidonoyl-PE (AA-PE) were increased in PMN-MDSC from cancer patients compared with PMN from healthy donors (Extended data Fig.8h). Thus, clinical data recapitulated the observations in mice.

Therapeutic targeting of FATP2

Next, we sought to determine the impact of the pharmacological inhibition of FATP2 on tumor growth. To inhibit FATP2 in TB mice, we used 5′-bromo-5-phenyl-spiro[3*H*-1,3,4-thiadiazole-2,3′-indoline]-2′-one, (lipofermata). This is a selective FATP2 inhibitor[15,25]. Lipofermata at the range of concentrations corresponding to the dose used *in vivo* (0.2 mg/ml) did not affect proliferation of EL-4 and LLC tumor cells *in vitro* (Extended data Fig. 9a). In four tested tumor models, lipofermata caused a significant delay of tumor growth (Fig. 4a). Notably this effect was absent in immune deficient SCID-NOD mice (Fig. 4b), and depletion of $CD8^+$ T cells in immune competent mice abrogated the effect of lipofermata (Fig. 4c). These data indicate that antitumor effect of FATP2 inhibition was mediated via immune mechanisms. In the TC-1 model, treatment with lipofermata increased the percentage and absolute numbers of antigen specific T cells in draining lymph nodes (Extended data Fig.9b).

We asked whether lipofermata could provide additional therapeutic benefit if combined with checkpoint inhibitors. Treatment of LLC bearing mice with lipofermata or CTLA4 alone had an antitumor effect. However, neither blocked tumor progression. In contrast, combination of CTLA4 antibody with lipofermata caused potent antitumor effect with 4 out of 5 mice rejecting tumors (Fig. 4d). A similar combination effect was observed in the TC1 model (Extended data Fig.9c). The antitumor effect was associated with substantial infiltration of $CD8^+$ T cells of tumors (Extended data Fig.9d). Combination of PD1 antibody with lipofermata in TC-1 model also resulted in significant decrease in tumor growth although this effect was less pronounced (Extended Fig. 9e). Since FATP2 is overexpressed only on PMN-MDSC, we asked whether the antitumor effects of lipofermata could be potentiated by combining with TAM targeted CSF1R antibody. Consistent with previous observations[26] CSF1R antibody alone had only a minor effect on tumor growth in the LLC tumor model. Combination of lipofermata with CSF1R antibody resulted in cellular antitumor effect (Fig. 4e).

Our study has identified FATP2 as a critical regulator of the immune suppressive function of PMN-MDSC, which mediates its effect via regulation of the accumulation of AA and subsequent synthesis of PGE2. These findings are consistent with the results demonstrating that production of PGE2 support tumor growth and immune escape[27]. Our study suggests a possibility of highly selective targeting of MDSC in cancer. Previous reports established the potential role of COX2 inhibitors in blockade of MDSC expansion in mouse tumor models[28,18,29,30]. However, prolonged systemic use of COX2 inhibitors is associated with substantial hematologic, cardiovascular and gastrointestinal toxicities. Selective targeting of FATP2 in PMN-MDSC offers the opportunity to inhibit PGE2 only in pathologically activated neutrophils and mostly within the tumor site, where expression of FATP2 is the highest. It is also possible that blockade of local release of PGE2 at the contact between PMN-MDSC and T cells in peripheral lymphoid organs can improve immune responses without systemic effects of PGE2 inhibition.

Methods

Human samples.

Samples of peripheral blood and tumor tissues were collected from patients at Helen F. Graham Cancer Center and University of Pennsylvania. The study was approved by Institutional Review Boards of the Christiana Care Health System at the Helen F. Graham Cancer Center, and The Wistar Institutional Review Board. All patients signed IRB approved consent forms. Samples were collected at Helen F. Graham Cancer Center from 6 patients with previously untreated stage II-IV non-small cell lung cancer (NSCLC), 11 patients with stage III-IV head and neck cancer and 5 patients with stage III-IV breast cancer. This cohort includes 12 females and 10 males, aged 48–74 years. Peripheral blood was also collected from 9 healthy volunteers after obtaining informed consent.

Mouse Models.

Animal experiments were approved by The Wistar Institute Animal Care and Use Committee. Balb/c or C57BL/6 mice (female, 6–8 week old) were obtained from Charles River, OT-I TCR-transgenic mice (C57Bl/6-Tg(TCRaTCRb)1100mjb) (female, 6–8 week old), B6.129S1-Cd36tm1Mfe/J, B6.Cg-Msr1tm1Csk/J, 129S-Slc27a2tm1Kds/J were purchased from Jackson Laboratory. C57Bl/6-Slc27a2tm1Kds/J were generated by backcrossing 129S-Slc27a2tm1Kds/J with wild type C57Bl/6 for ten generations. B6.129S6-Stat5^{btm1Mam} Stat5atm2$^{Mam/Mmjax}$ were crossed with B6.Cg-Tg(S100A8-cre,-EGFP)1Ilw/J, obtained from Jackson Laboratory. RET melanoma were obtained from Dr. Umansky (German Cancer Center, Heidelberg, Germany). *Scl27a4*$^{fl/fl}$ were obtained from Dr. Stremmel (University of Heidelberg, Germany) and crossed with B6.Cg-Tg(S100A8-cre,-EGFP)1Ilw/J (Jackson Laboratory). In mouse tumor models maximal tumor size approved by IACUC was 2 cm in larger diameter. In none of the experiments were these limits exceeded. Sample size calculation was performed in advance. Studies were not blinded. In treatment experiments, mice were randomized prior to start of therapy to different groups based on equal tumor size.

Generation of PMN-specific SLC27A2-deficient mice.

Mice were generated at CRISPR/Cas9 Mouse Targeting Core of University of Pennsylvania, using the CRISPR/Cas9 system as described[31]. Conditional knock-out mice (CKO Scl27a2$^{fl/fl}$) were generated using CRISPR-Cas9 genome-editing system, at CRISPR Cas9 Mouse Targeting Core of University of Pennsylvania by flanking Exon 1 with loxp sites, as described[31]. The sequences for the gRNAs and repair templates used are as follows: Slc27a2 5'gRNA: GTCCACAATACCGTCGATGTGTTTTAGAGCTAGAAATAGCAAGTTAAAATAAGGCTAGTCCGTTATCAACTTGAAAAAGTGGCACCGAGTCGGTGCTTTTTT. Slc27a2 3' gRNA: ACTCCTCCGTTATATGATTGGTTTTAGAGCTAGAAATAGCAAGTTAAAATAAGGCTAGTCCGTTATCAACTTGAAAAAGTGGCACCGAGTCGGTGCTTTTTT. Slc27a2 5' LoxP oligoDNA:TTTACTTTGTTTGCTTTGTGTGTTTTGGTAAATGTCGAACTGAGTCCACAATACCGTCGATGTataacttcgtataatgtatgctatacgaagttatTGGAAAGTGGCTCGCGTAACAGAACAAAATCTCAAAACAAATTAACAGGACCCCATTGCTCGA. Slc27a2 3' LoxP

oligoDNA: ATACTGTAATGGATGGTTTTAATATTCTGATAAATTAAAAATCACTCCTCCGTTATATGATTGataacttcgtataatgtatgctatacgaagttatAGGAAACATATAGAATTTTCCAGCCTAGCTCCGTCTTCAAAGCCCACGTTTCTTATACAGTGC. Scl27a2$^{fl/fl}$ mice were then crossed with B6.Cg-Tg(S100A8-cre,-EGFP)1Ilw/J (Jackson Laboratory) to obtain mice with targeted deletion of FATP2.

Reagents and cell lines.

Tumor cell lines: EL4 (lymphoma), LLC (Lewis Lung Carcinoma), CT26 (colon carcinoma), TC-1 (HPV16 E6/E7 expressing tumor cell line) were obtained from ATCC and F244 (sarcoma) was kindly provided by Dr. R. Schreiber (Washington University, St. Lois, MO). All cells were maintained in DMEM medium supplemented with 10% fetal bovine serum (FBS, Sigma-Aldrich, St. Louis, MO) at 37 °C, 5% CO2. Tumor cells were injected subcutaneously (s.c.) at 5×10^5 cells per mouse. Tumor cell lines were obtained from ATCC and were tested for mycoplasma contamination by using Universal Mycoplasma detection kit (ATCC) every 3 months. SIINFEKL and EGSRNQDWL peptides were obtained from American Peptide Company (Vista, CA). All reagents and antibodies used in the study are described in Supplemental Table 1.

Preparation of TES.

Tumor explant supernatants (TES) were prepared from excised non-ulcerated EL4 tumors ~1.5 cm in diameter. A small tumor piece (5–10 mm^2) was harvested, minced into pieces <3 mm in diameter and resuspended in complete RPMI without extra cytokines. After 16–18 hours of incubation at 37 °C with 5% CO_2, the cell-free supernatant was collected using 0.22 μm filters (EMD Millipore) and kept at −80 °C.

Cell phenotype, lipid contents by flow cytometry and by confocal microscopy.

Cells were incubated with FC-block (BD Biosciences) for 10 min and surface staining was performed at 4°C for 15 min. Cells were run on LSRII flow cytometer (BD Biosciences) and data were analyzed by FlowJo (Tristar). For lipid staining by flow cyometry, cells were re-suspended in 500 μl of Bodipy 493/503 at 0.25 μg/ml in PBS. Cells were stained for 15 min at room temperature in the dark, then washed twice, re-suspended in PBS and run immediately on LSRII. For lipid staining by confocal microscopy, cells were washed twice with PBS, resuspended in complete RPMI and 50,000 cells were seeded on poly-L-lysine cellware 12 MM round coverslips (Corning) for 45 min at 37 °C. Cells were fixed and permeabilized with Fixation & Permeabilization Buffers (BD Biosciences) for 15 min at RT, washed twice with wash buffer (BD Biosciences) and then stained with BODIPY for 15 min at RT. Cells were washed and incubated with DAPI and mounted on slides using Prolong Gold antifade reagent (Life Technology). The cells were imaged with a Leica TCS SP5 laser scanning confocal microscope (Leica Microsystems).

Isolation of mouse cells.

Single-cell suspensions were prepared from spleen and followed by red blood cell removal using ammonium chloride lysis buffer. Single-cell suspensions from tumor tissues were

prepared using Mouse Tumor Dissociation Kit according to the manufacturer's recommendation (Miltenyi). $CD8^+$ T cells were isolated from spleen and lymph nodes by using EasySep Mouse $CD8^+$ T Cell Enrichment Kit (STEMCELL), following manufacturer's instructions.

Suppression assay.

Single cells suspensions from spleen and tumors were prepared as described above. Then cells were stained and sorted on BD FACS Aria BD (Biosciences). PMN-MDSC ($CD45^+CD11b^+Ly6G^+Ly6C^{lo}$) and M-MDSC ($CD45^+$ $CD11b^+Ly6G^-Ly6C^{hi}$) were plated in U-bottom 96-well plates (3 replicates) in RPMI with 10% FBS and co-cultured at different ratios with splenocytes from Pmel or OT-1 transgenic mice in the presence of cognate peptides: OT-1 (SIINFEKL; 0.1 ng/ml), Pmel (EGSRNQDWL; 0.1 μg/ml). After 48 h, cells were incubated with [^{3}H]-thymidine (PerkinElmer) for 16–18 h. Proliferation was measured by using TopCount NXT instrument (PerkinElmer).

IFNγ ELISpot, T cell proliferation and antigen specific T cell analysis.

Lymph nodes (LNs) were obtained from TB mice and digested for 30 min at 37 °C with collagenase A (0.5 mg/ml; Sigma Aldrich), Dnase I (0.2 mg/ml, Roche), diluted in HBSS with Ca^{2+}/Mg^{2+} and 20mM EDTA (Invitrogen) was added 5 min at room temperature to stop the reaction. CD8 T cells were isolated from LNs of TB mice using EasySep Mouse $CD8^+$ T Cell Enrichment Kit (STEMCELL) and stimulated with anti CD3 and anti CD28 antibodies (BD Biosciences) for 24h and IFNγ was analyzed by ELISpot (Mabtech), accordingly to manufacturer's instructions. T cell proliferation was evaluated by flow cytometry using CSFE (BioLegend). Antigen specific CD8 T cell response was evaluated in single cell suspension obtained from LNs of TC1 (HPV16 E6/E7 expressing tumor cells) TB mice by flow cytometry using MHC tetramer (H-2Db HPV 16 E7 – RAHYNIVTF), obtained from D. Weiner (Wistar Institute, Philadelphia, USA).

Isolation of human cells.

PMN-MDSC and PMN were isolated by centrifugation over a double density gradient Histopaque (Sigma) (1.077 to collect PBMC and 1.119 to collect PMN) followed by labeling with CD15-PE mAb (BD Biosciences) and then separated using anti-PE beads and MACS column (Miltenyi). Tissues were first digested with human tumor dissociation kit (Miltenyi) and then red blood cell lysed. Cells were then culture in RPMI (Biosource International) supplemented with 10% FBS, 5 mM glutamine, 25 mM HEPES, 50μM β-mercaptoethanol and 1% antibiotics (Invitrogen). For isolation of $Lox1^+$ PMN from peripheral blood, whole blood was enriched for PMNs using MACSxpress® Neutrophil Isolation Kit (Miltenyi) following the protocol provided by the manufacturer. Cells were then labeled with anti-Lox1-PE mAb (Biolegend) and then separated using anti-PE beads and MACS column (Miltenyi).

Quantitative real time PCR.

RNA was extracted using Total RNA Kit according to manufacturer's instructions. DNase digestion was performed cDNA was generated with High-Capacity cDNA Reverse

Transcription Kit (Applied Biosystems, Foster City, CA, USA). qRT-PCR was performed using Power SYBR Green PCR Master Mix (Applied Biosystems) in 96- or 384 well plates. Plates were read with ABI 7900 (Applied Biosystems). Amplifications were carried out with the primers described in Supplemental Table 2.

RNA-seq.

RNA-seq data was aligned using bowtie2[32] against mm10 version of the mouse genome and RSEM v1.2.12 software[33] was used to estimate raw read counts using Ensemble v84 gene information. DESeq2[34] was used to estimate significance of differential expression between sample groups. Overall gene expression changes were considered significant if passed false discovery rate FDR<5% threshold. Significant genes affected at least 2 fold were analyzed for enrichment of upstream regulators using QIAGEN's Ingenuity® Pathway Analysis software (IPA®, QIAGEN Redwood City,www.qiagen.com/ingenuity, "Upstream Analysis" option). Only regulators with significantly enriched $p<0.005$ targets (at least 20) with significantly predicted activation state (activation z-score $|Z|>2$) were considered.

Western blot.

Cells were lysed in RIPA buffer (Sigma-Aldrich) in presence of protease inhibitor cocktail (Sigma-Aldrich), sonicated and stored at −80°C. Whole cell lysates were prepared and subjected to 10% SDS-PAGE and transferred to PVDF membrane. The membranes were probed overnight at 4°C with the antibodies specific for FATP2 (SLC27A2) (ThermoFisher), ACTIN, GAPDH, STAT5 (Cell Signaling Technology). Membranes were washed and incubated for 1 h at room temperature with secondary antibody conjugated with peroxidase.

Generation of suppressive neutrophils *in vitro*.

Mouse neutrophils were generated from enriched bone marrow hematopoietic progenitor cells (HPCs) with 20 ng/ml of GM-CSF. Briefly, HPCs were isolated from mouse BM by using Lineage depletion kit (Miltenyi), according to manufacturer's instructions. Cells were seeded at 25000 cell/ml in 24 well plates and GM-CSF (20 ng/ml), 20% v/v TES or arachidonic acid (10μM) were added at day 0 and day 3. At day 5, Ly6G positive neutrophils were isolated by using anti-Ly6G biotin (Miltenyi) and streptavidin beads (Miltenyi), according to manufacturer's instructions.

FATP2 overexpression in HPC and PGE2 ELISA.

HPCs were isolated from mouse BM by using Lineage depletion kit (Miltenyi), according to manufacturer's instructions. HPC were resuspended in serum-free medium (SFM) containing lentiviral vectors followed by centrifugation of the plate at 1000 rpm for 20 min at 25°C. Fresh media supplemented with GM-CSF (20 ng/ml) was then added and cells were seeded at 25000 cell/ml in 24 well plates. At day 3, GM-CSF and 20% v/v TES were added to the culture. At day 5, cells were collected, stained with PE conjugated anti mouse Ly6G, APC conjugated anti mouse Ly6C and BV421 conjugated anti-mouse CD11b, and GFP- and GFP^+ $Ly6G^+$ cells were sorted on BD FACS Melody (BD Biosciences). GFP^- and GFP^+ $Ly6G^+$ cells were seeded at 2.000.000 cells/ml in presence of GM-CSF and TES and incubated for further 24 hours. Pellets and supernatants were collected for further analysis.

PGE2 concentration in supernatants was measured by using PGE2 ELISA KIT (Invitrogen), according to manufacturer's instructions.

Uptake and tracing of arachidonic acid.

Splenic PMN-MDSC from WT and FATP2 KO LLC TB mice were cultured in complete media (RPMI+10%FBS) with 100 nM of d11AA (Cayman Chemicals), conjugated to 10% fatty acid-free BSA (Sigma Aldrich), and 10 ng/ml of GM-CSF. After 16–18h, supernatants and cellular pellets were collected and stored at −80c. Lipids (including PGE2 and PGE2d11) were analyzed by LC-MS; the amounts of PGE2 in the supernatants were measured by ELISA.

Immunofluorescence microscopy.

Immunofluorescence staining of CD8 was performed on frozen mouse tumor tissue sections. Rat monoclonal anti-mouse CD8a primary antibody (BD Pharmingen™) and Alexa Fluor 594 goat anti-rat IgG (H+L) secondary antibody (Invitrogen) were used for the staining. Cell nuclei were stained with DAPI. Imaging was performed using a Leica TCS SP5 confocal microscope. Sixteen frames acquired with a 63X objective lens were used to calculate the cell number per mm^2.

Seahorse analysis.

Metabolic rates were determined using the Seahorse XFe24 and XFe96 Flux Analyzers (Agilent Technologies) following the manufacturer's protocol. Briefly, the microplate was coated with 22.4 μg/ml Cell-Tak (Fisher) using 200mM sodium bicarbonate. 400,000 cells were seeded per well immediately after isolation in 50μl and 80μl of unbuffered RPMI (Sigma-Aldrich) for the XF24 and XF96 analyzers, respectively. The microplate was incubated for 30 min at 37°C to allow the cells to settle into a monolayer. Unbuffered RPMI was gently added to the wells without disturbing the monolayer to bring the assay volume to 675μl and 180μl for the XFe24 and XFe96 analyzer, respectively. The basal oxygen consumption rate (OCR) and extracellular acidification rate (ECAR) was measured, in addition to rate changes upon treatment with 5μM oligomycin (Sigma-Aldrich), 1μM FCCP (Sigma-Aldrich), and 0.75μM rotenone and 1μM antimycin A (Sigma-Aldrich).

Chromatin immunoprecipitation (ChIP)

Chromatin immunoprecipitation (ChIP) assays were performed as described previously[35]. Briefly, PBMC cells were treated or not with GM-CSF 10ng/ml and 100ng/ml for 20 min. Cells then were fixed in 1% formaldehyde for 10 min. DNAs were sonicated to obtain 200- to 400-bp DNA fragments on a Diagenode Bioruptor according to the manufacturer's protocol. The following antibodies were used for ChIP assays: anti-rabbit IgG (Santa Cruz Biotechnology), anti-Phospho-STAT5 alpha (Tyr694) Antibody (6H5L15) Rabbit Monoclonal (Invitrogen). Primers for ChIP assays are listed in Supplemental Table 2. PCR data were normalized to input values that were quantified in parallel for each experiment.

Tumor cell injections and treatment.

5×10^5 tumor cells were injected s.c. into mice, which formed tumors with a 1.5-cm diameter within 2–3 weeks of injection. Lipofermata was administrated s.c. at dose of 2 mg/kg twice per day. As a control, mice were treated with vehicle alone (DMSO + 30% v/v Kolliphor). Treatments with lipofermata started 8–10 days after tumors injections. CSF1R antibody (BioXcell, 300 μg/mouse) was administered every other day starting next day after tumor injection and continued until the mice were sacrificed. PD-1 antibody (clone RMP1–14, BioXcell, 200 μg/mouse) was administered twice a week started 10–12 days after tumor injection. CTLA4-IgG2a (BioXcell, 200 μg/mouse) was administered at day 7 and day 11.

Liquid chromatography-mass-spectrometry of lipids.

Lipids were extracted by Folch procedure with slight modifications, under nitrogen atmosphere, at all steps. The detailed protocol is provided in Supplemental Experimental Procedures. LC/ESI-MS analysis of lipids was performed on a Dionex HPLC system (utilizing the Chromeleon software), consisting of a Dionex UltiMate 3000 mobile phase pump, equipped with an UltiMate 3000 degassing unit and UltiMate 3000 autosampler (sampler chamber temperature was set at 4°C). The Dionex HPLC system was coupled to an Orbitrap Fusion Lumos mass spectrometer (ThermoFisher Scientific) or to a hybrid quadrupole-orbitrap mass spectrometer, Q-Exactive (ThermoFisher, Inc., San Jose, CA) with the Xcalibur operating system. The instrument was operated in negative and positive ion modes (at a voltage differential of –3.5–5.0 kV, source temperature was maintained at 150°C). Phospholipids (PLs) MS and MS/MS analysis was performed on an Orbitrap Fusion Lumos mass spectrometer. The details are provided in Supplementary Information. MS and MS/MS analysis of free fatty acids (FFA) and TAG/CE was performed on a Q-Exactive hybrid-quadrupole-orbitrap mass spectrometer (ThermoFisher, Inc. San Jose, CA). The details are provided in Supplementary Information. MS lipid standards were from Avanti Polar Lipids (Alabaster, AL) and from Cayman Chemical Company (Ann Arbor, MI). Analysis of LC-MS data was performed using the software package Compound Discoverer™ (ThemoFisher Scientific).

Construction of LV-GFP-FATP2 plasmid.

The FATP2 gene was amplified from the pCMV6-Kan/Neo-FATP2 plasmid (Origene, Cat# MC206275) using the following primers: FATP2_For_XmaI (GGTGGTCCCGGGCCTATGCTGCCAGTGCTCTACAC) and FATP2_Rev_SalI (GGTGGTGTCGACTCAGAGCTTCAGAGTTTTAT). The amplified PCR product was then digested with *XmaI/SalI* and cloned into a SIV-based self-inactivating lentiviral transfer vector downstream of GFP (pGAE-CMV-GFP-P2A-FATP2-Wpre). The transfer vector pGAE-CMV-GFP-Wpre, the packaging plasmid pAd-SIV3+, and the vesicular stomatitis virus envelope G protein (VSV-G) pseudotyping vector from Indiana serotype (pVSV.G_{IND}), have been previously described[36,37]. Vector production and validation is described in Supplemental Information.

Statistical analysis.

Statistical analysis was performed using unpaired two-tailed Student's *t*-test with significance determined at 0.05. Estimation of variation within each group of data was performed and variance was similar between groups that were compared. Animal experiments were not blinded. Tumor growth was evaluated using two-way Anova test with Bonferroni correction for multiple comparisons.

Extended Data

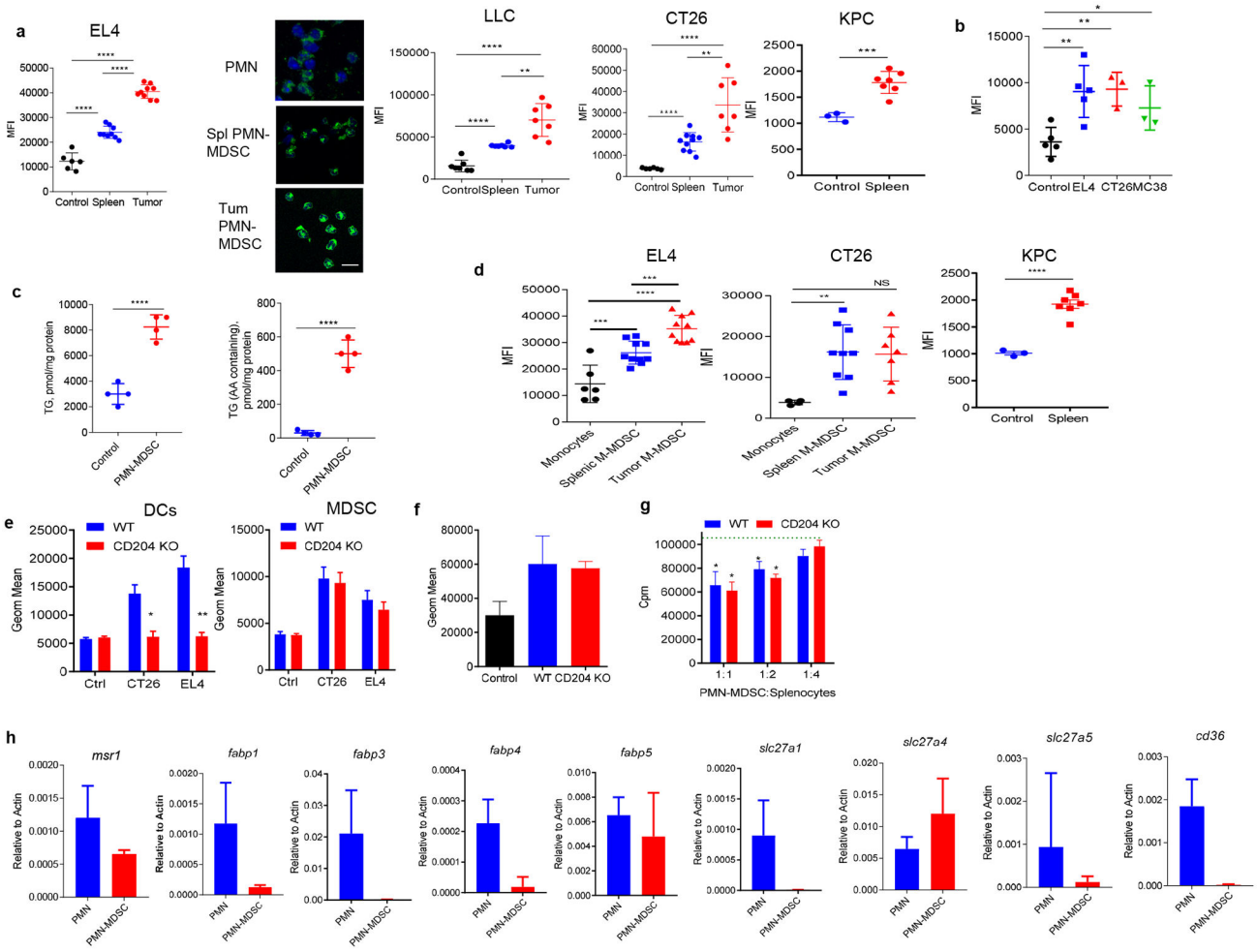

Extended data Figure 1. Lipid accumulation and expression of lipid transporters in MDSC

a. Lipid accumulation measured by BODIPY staining in PMN-MDSC isolated from spleen and tumors of indicated tumor models. Each group included 4–8 mice. Each circle represents an individual mouse. Mean ± SD are shown. Inset - confocal image representative of 2 independent experiments. **b.** Lipid accumulation in PMN generated from BM HPC with GM-CSF and TES. (n=3–5). **c.** LC/MS analysis of TG in PMN from control mice and PMN-MDSC from of EL4 TB mice (n=4). **d.** Lipid accumulation measured by BODIPY staining in M-MDSC isolated from spleen and tumor of indicated tumor models (n=10). Each circle represents an individual mouse. Mean ± SD are shown. **e.** Lipid accumulation in DC and MDSC generated from CD204 KO HPC in presence of TES (n=3). Mean ± SD are shown. **f.** Lipid accumulation in PMN-MDSC from spleen of tumor bearing WT and CD204 KO mice (n=3). Mean ± SD are shown. **g.** Suppressive activity of PMN-MDSC from spleen of tumor bearing WT and CD204 KO mice. Representative of 4 experiments each performed in triplicates. Mean ± SD are shown. **h.** Expression of *msr1, fabps, slc27a (1–5), cd36* in control PMN and PMN-MDSC isolated from spleen and tumor of EL4 TB mice (n=4–5). Mean ± SD are shown. In all panels, p values were calculated in unpaired two-sided Student's *t*-test: *P<0.05; **P<0.01; ***P<0.001; ****P<0.0001.

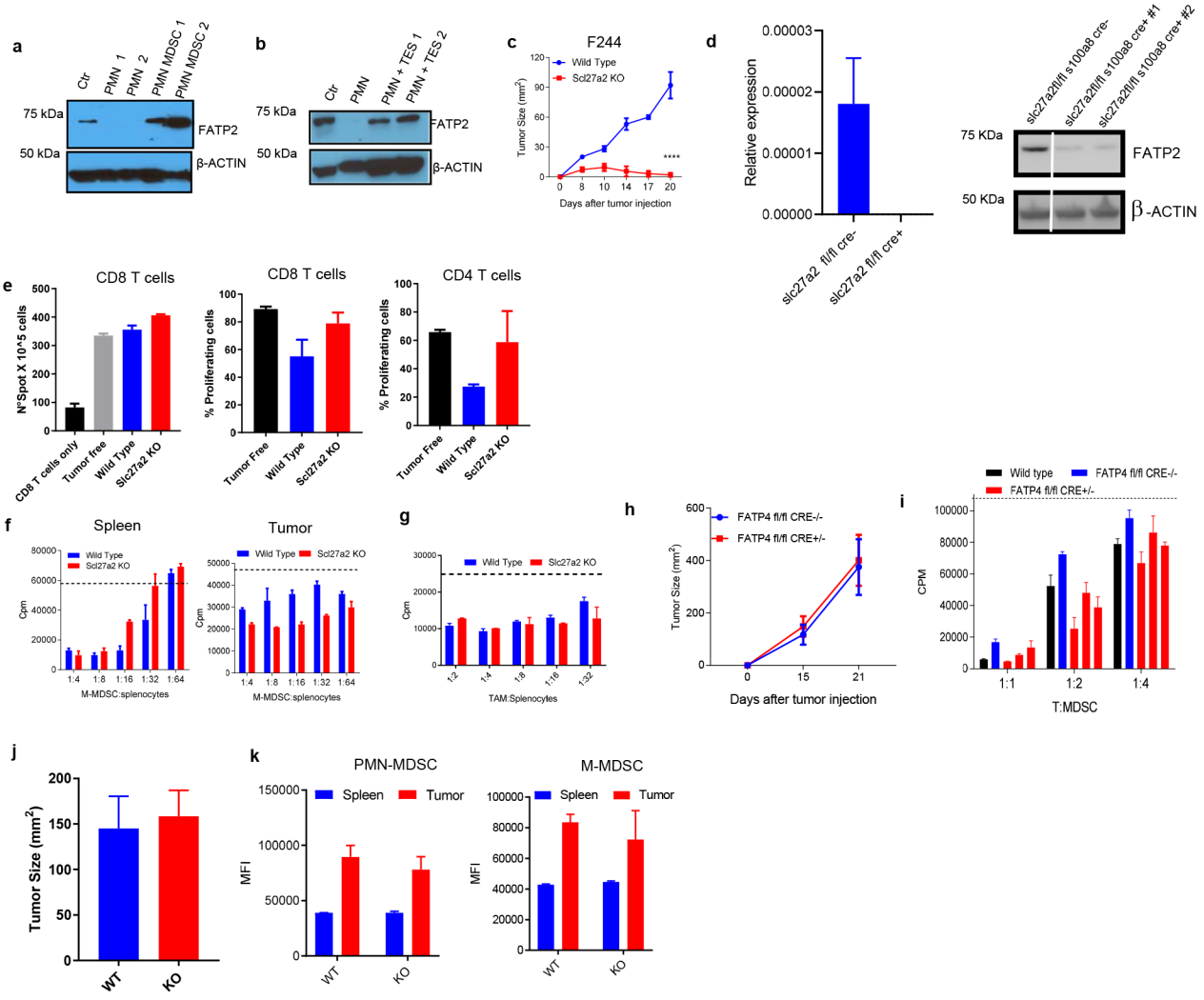

Extended data Figure 2. Expression of gene involved in lipogenesis in PMN-MDSC.

a. FATP2 protein in control PMN and PMN-MDSC from spleen of TB mice. Representative of 2 experiments. **b.** FATP2 in PMN generated *in vitro* from BM HPC. Representative of 2 experiments. For gel source data, see Supplementary Figure 1. **c.** F244 tumor growth in WT and FATP2 KO SV129veve mice (n=4). **d.** Verification of correct targeting of FATP2 by RT-qPCR and WB in PMN-MDSC isolated from spleen of *slc27a2*$^{fl/fl}$ x *s100a8-cre*$^{-}$ and *slc27a2*$^{fl/fl}$ x *s100a8-cre*$^{+}$ TB mice. For gel source data, see Supplementary Figure 1. **e.** IFNγ production by CD8^{+} T cells and CD4 and CD8 T-cell proliferation (n=3) in WT and FATP2KO mice. Mean ± SD are shown. **f.** Suppressive activity of M-MDSC isolated from WT or FATP2 KO TB mice. Dashed line shows T cell proliferation without MDSC. Four experiments with similar results were performed. **g.** Suppressive activity of TAM from WT or FATP2 KO TB mice. Dashed line shows T-cell proliferation without macrophages. 3 independent experiments with similar results were performed. In all panels mean and SD are shown. **h.** Growth of EL4 tumors in WT and FATP4 KO mice (n=4). Representative of 2 experiments. Mean ± SD are shown. **i.** Suppressive activity of PMN-MDSC isolated from spleen or tumor of WT or FATP4 KO mice. Representative of 2 independent experiments

performed in triplicates. Mean ± SD are shown. Dotted line – control values of T cell proliferation without presence of PMN-MDSC. **j.** Growth of LLC tumor in WT and CD36 KO mice, depleted of $CD8^+$ T cells (n=3). Mean ± SD are shown. **k.** Lipid accumulation measured by BODIPY staining in PMN-MDSC and M-MDSC isolated from spleen and tumor of CD36 KO mice (n=3). Mean ± SD are shown. In all experiments p values were calculated in unpaired two-sided Student's *t*-test.

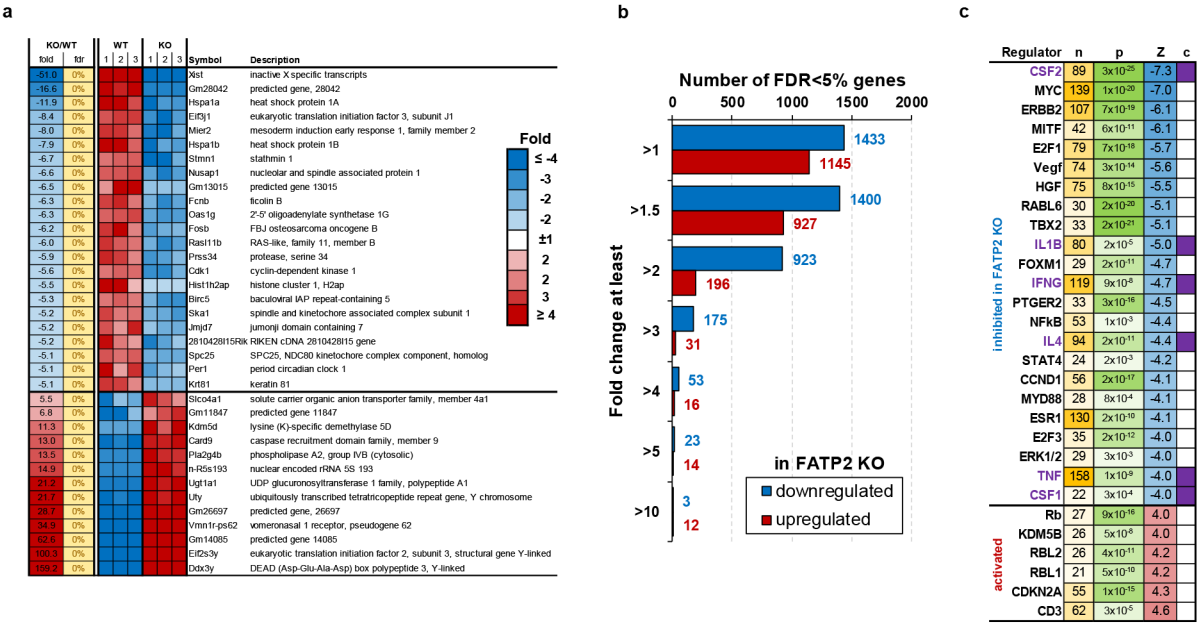

Extended data Figure 3. Effect of FATP2 KO on mRNA gene expression.

a. Expression heatmap for genes affected at least 5-fold, **b.** Number of significantly affected genes (FDR<5%) for different fold change thresholds. **c.** List of upstream regulators whose targets were found by Ingenuity Pathway Analysis (IPA) as significantly enriched among genes affected by FATP2 KO. n=number of affected targets, p=enrichment pvalue, Z=activation z-scores calculated by IPA represent predicted regulator state based on the known effect on target and direction of mRNA change. Negative activation z-scores predict inhibition and positive z-scores – activation of the regulator in the FATP2 KO mice.

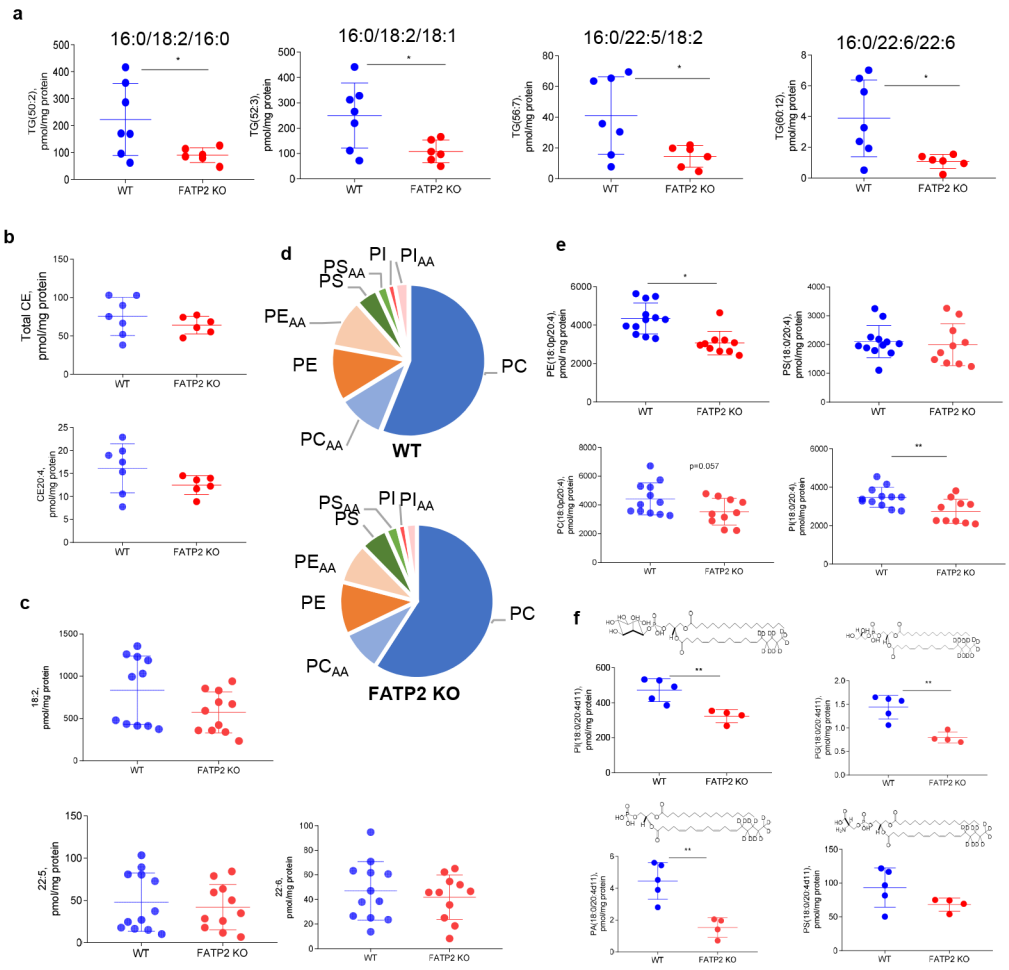

Extended data Figure 4. LC-MS analysis of lipids from WT and FATP2 KO PMN-MDSC.
a. TGs molecular species containing LA (18:2), docosapentaenoic acid (22:5), and docosahexaenoic acid (22:6) **(**n=7)**. b.** Total CE and CE (20:4) molecular species (n=7). **c.** LA (18:2), docosapentaenoic acid (22:5), and docosahexaenoic acid (22:6) fatty acids (n=12). **d.** Distribution of major PLs in FATP2 KO and WT PMN-MDSC samples. **e**. Content of PLs containing AA in PE, PC, PI, and PS (n=12). **f.** Content of AAd11 labelled phospholipids (PI, PG, PA and PS), n=5. Statistical analysis was performed using unpaired two-sided Student's t-test *P<0.05; **P<0.01 (each circle indicates an individual mouse, Mean ± SD).

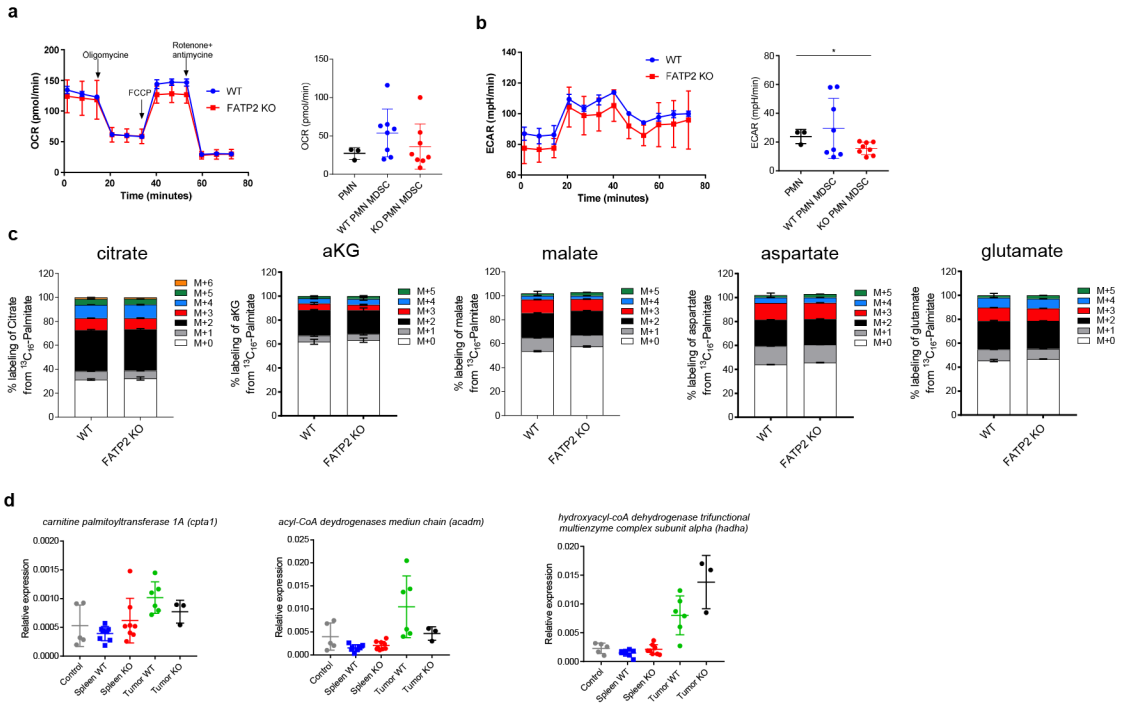

Extended data Figure 5. Metabolomic analysis and expression of FAO related genes in PMN-MDSC.

a. Oxygen consumption rate (OCR) (top panel) and basal OCR (bottom panel) of WT and FATP2 KO PMN-MDSC. Representative of 2 experiments is shown in top panel (n=3–4). Bottom panel cumulative results are shown. Each circle indicates an individual mouse (n=7). Mean and SD are shown. P values were calculated using unpaired two-sided Student's t-test. **b**. Extracellular acidification rate (ECAR) (top panel) and basal ECAR (bottom panel) of WT and FATP2 KO PMN-MDSC. Top panel - representative of 2 independent experiments (n=3–4). Bottom panel – cumulative results. Each circle indicates an individual mouse (n=7). Mean and SD are shown. Statistical analysis (unpaired two-sided Student's t-test) was performed. NS, not significant; *P<0.05. **c**. Carbon-13 labeling of TCA cycle intermediates and associated amino acids. *Ex vivo* MDSC were cultured in physiological-like medium supplemented with BSA-conjugated 13C16-palmitate and GM-CSF for 18 hours. Metabolites were then extracted and analyzed by high-resolution LC-MS. Carbon-13 isotopologs (M+x) for each metabolite are represented as normalized stacked bars. Data presented as Mean and SD of 3 biological replicates. Statistical analysis (unpaired two-sided Student's t-test) was performed. **d.** Expression of genes involved in FAO. RT-qPCR analysis of *cpta1, acadm, hadha* expression in control PMN and PMN-MDSC isolated from spleen and tumor of TB mice. Each group included 3–6 mice and shown as Mean ± SD

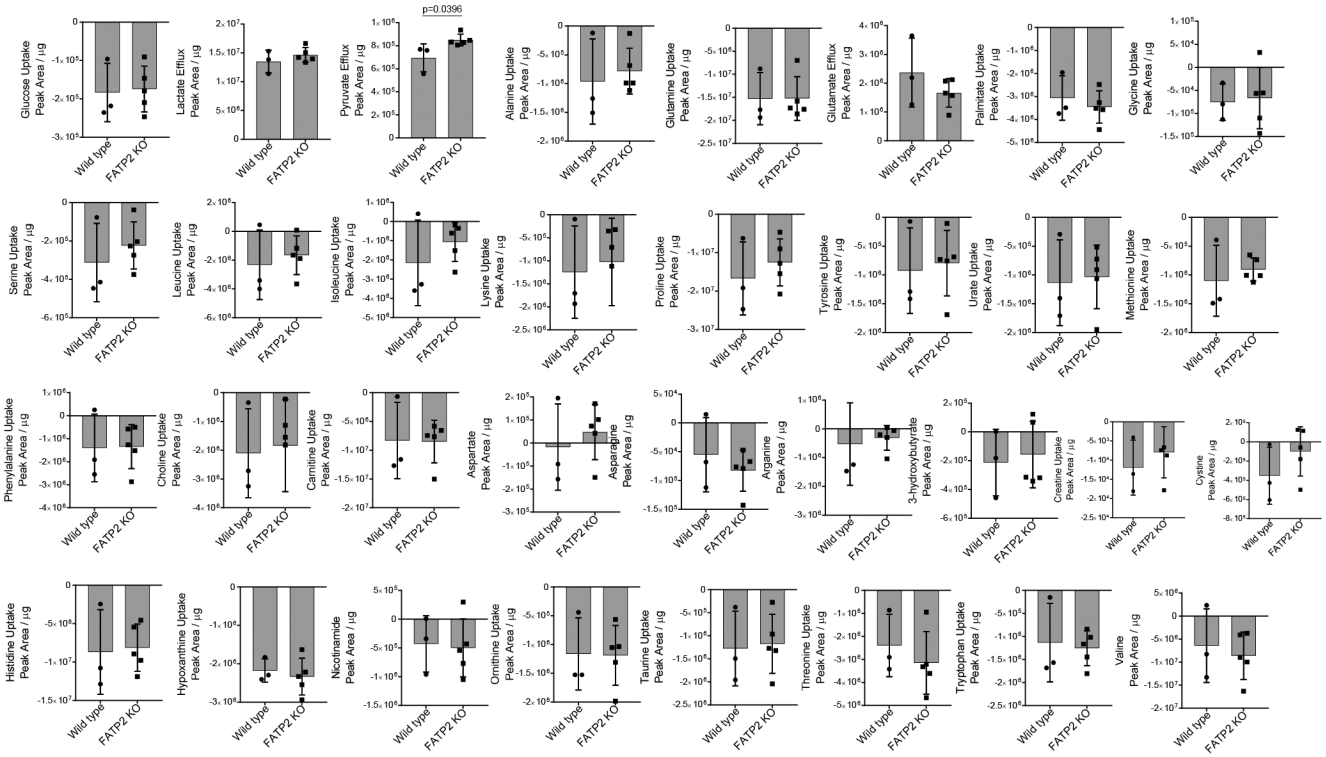

Extended data Figure 6. Exchange of nutrients with the media.

Ex vivo MDSCs were cultured in physiological-like medium supplemented with GM-CSF for 18 hours. Metabolites were then extracted from the media and analyzed by LC-MS. Upward bars represent efflux from the cells into the media, and downward bars represent uptake (or depletion) from the media by the cells. Data are normalized to protein content after extraction. Data are presented as a mean and SD (n=3).

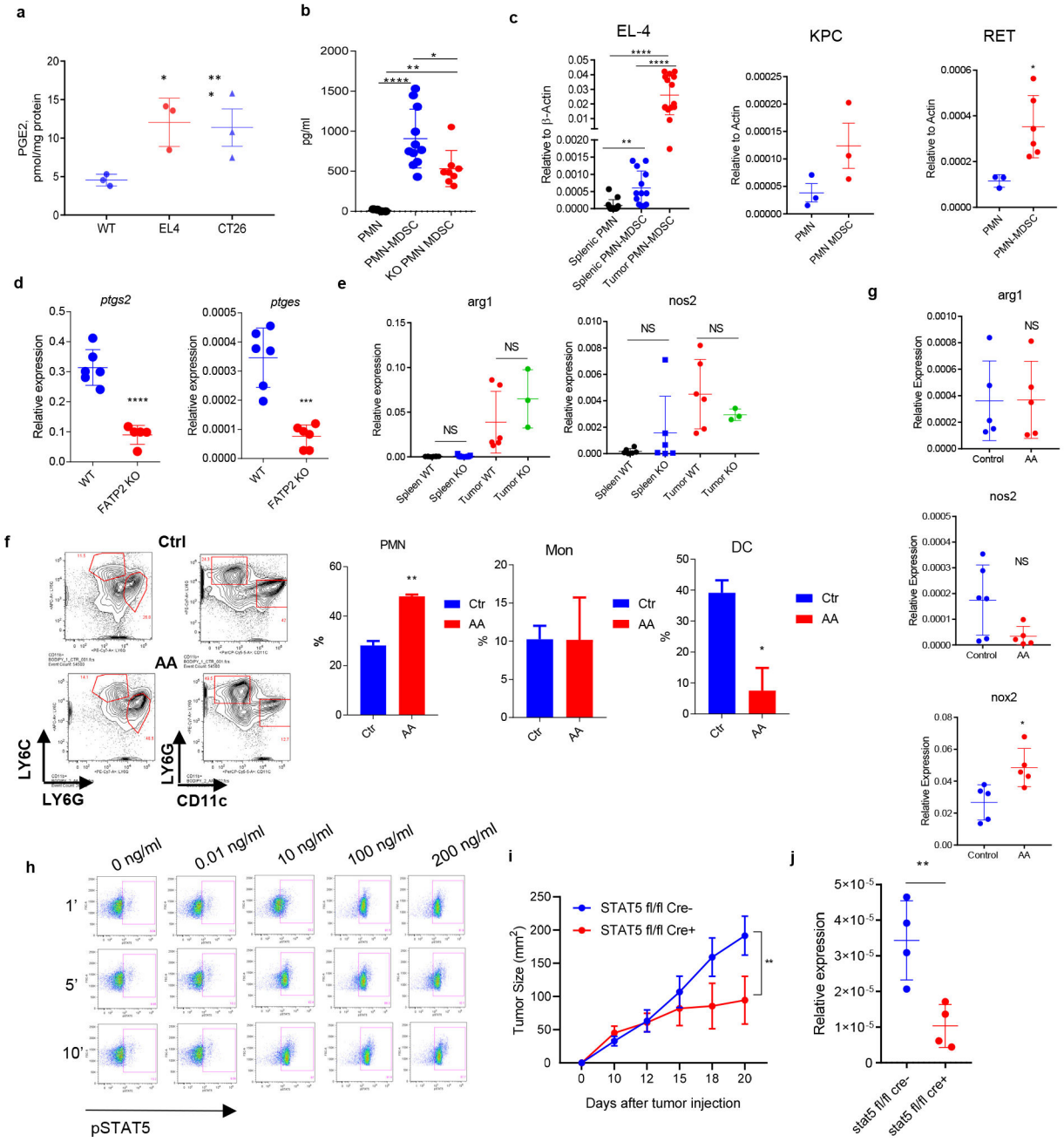

Extended data Fig. 7. Effect of AA on PGE2 production and suppressive activity of PMN-MDSC.

a. LC/MS analysis of PGE2 in PMN from control mice and PMN-MDSC from EL4 and CT26 TB mice (n=3). Mean ± SD are shown. **b.** PGE2 release (ELISA) by control PMN (n=4), PMN-MDSC from WT (n=11), and FATP2 KO (n=8) LLC TB mice. **c.** Expression of *ptges* in PMN-MDSC isolated form spleen of EL4 TB mice (n=13–15), KPC (n=3), RET (n=3–6). Mean ± SD are shown. **d.** Expression of *ptgs2* and *ptges* in PMN-MDSC (qRT-PCR) (n=6). **e.** Expression of *arg1* and *nos2* (qRT-PCR) in spleen PMN-MDSC from WT and FATP2 KO EL4 TB mice (n=3–5). Mean ± SD are shown. **f.** Flow cytometry of myeloid cells differentiated from HPC in presence of AA. Representative of 3 experiments. **g.**

Expression of *arg1, nos2* and *nox2* in PMN isolated from HPC cultures with AA. Data are pooled from 6 independent experiments and depicted as mean ± SD. **h.** pSTAT5 by flow cytometry at different time points in mouse PMN isolated from BM treated with different amounts of GM-CSF. Representative of 3 independent experiments. **i.** LLC tumor growth (n=4) in *stat5*$^{fl/fl}$:cre^{-} and *stat5*$^{fl/fl}$:cre^{+} mice. **j.** *Slc27a2* expression (RT-qPCR) in PMN-MDSC from spleen of WT and KO TB mice (n=4). Statistical analysis - unpaired two-sided Student's *t*-test: NS, not significant; *P<0.05; **P<0.01

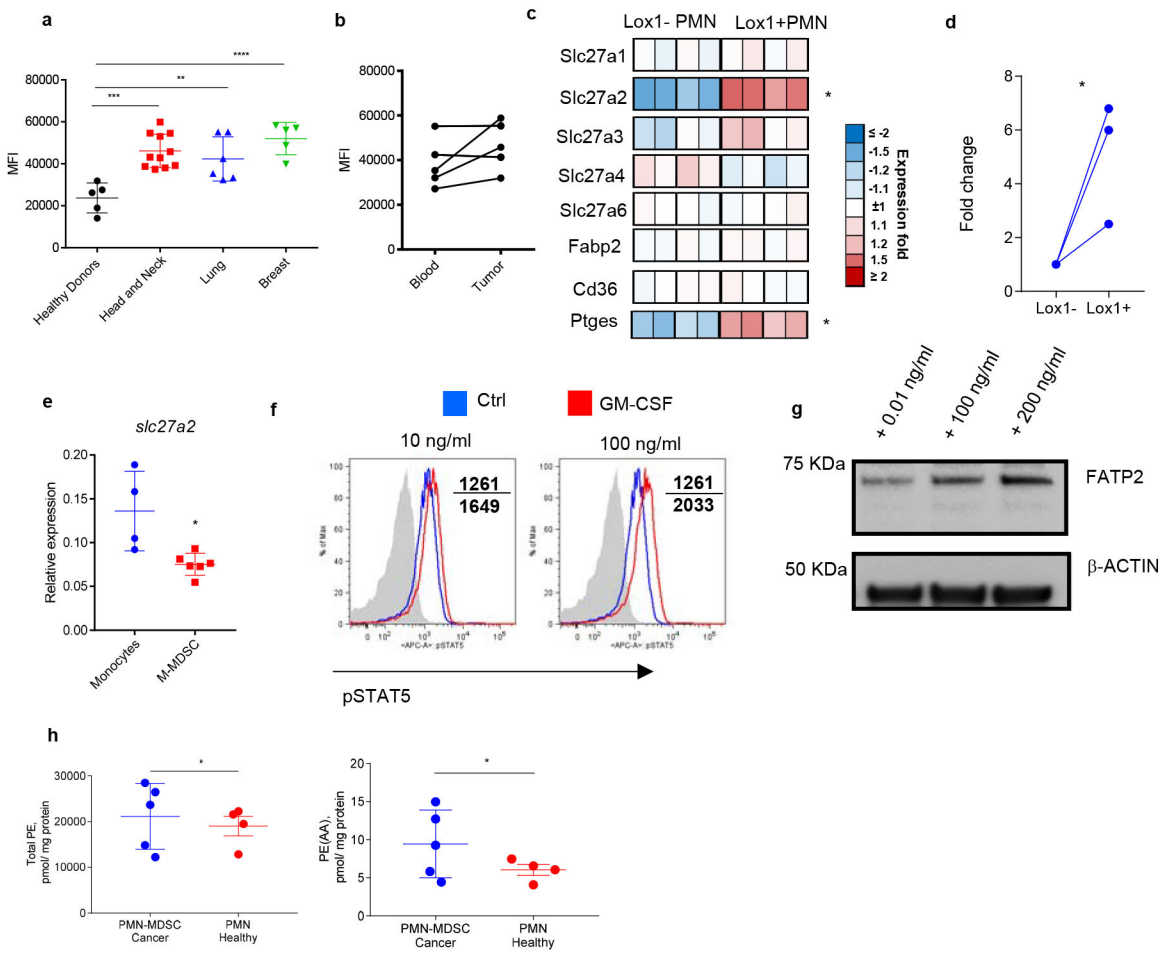

Extended data Figure 8. Lipid accumulation in MDSC from cancer patients.

a. Amount of lipids (BODIPY staining) in M-MDSC isolated from blood of cancer patients or healthy individuals. Each circle indicates an individual and Mean ± SD are also shown. **b.** Amount of lipids (BODIPY staining) in M-MDSC from blood and tumor tissue of cancer patients. Each circle indicates an individual (n=5). **c**. RNAseq analysis of genes involved in lipid accumulation in human LOX1^{+} PMN-MDSC and LOX1^{-} PMN (n=4). **d.** *PTGES* expression in LOX1^{+} and LOX1^{-} PMN from blood of cancer patients. Fold change over LOX1^{-}PMN (n=3). **e.** *Slc27a2* expression in M-MDSC and monocytes isolated from blood of cancer patients and healthy donors, respectively. Each circle indicates an individual (n=4–6). Mean ± SD are shown. **f.** pSTAT5 by flow cytometry at different time points, in human PMN isolated from blood of healthy donor and treated with different amounts of GM-CSF. **g.** FATP2 in PMN isolated from blood of healthy donors and treated with GM-CSF. Representative of 3 independent experiments is shown. For gel source data, see Supplementary Figure 1. **h.** Content of total PE and AA-containing PE species in PMN-MDSC isolated from lung cancer patients or healthy donors. Each circle indicates an individual; mean ± SD (n=4). Statistical analysis - unpaired two-sided Student's *t*-test: *P<0.05; **P<0.01; ***P<0.001; ****P<0.0001.

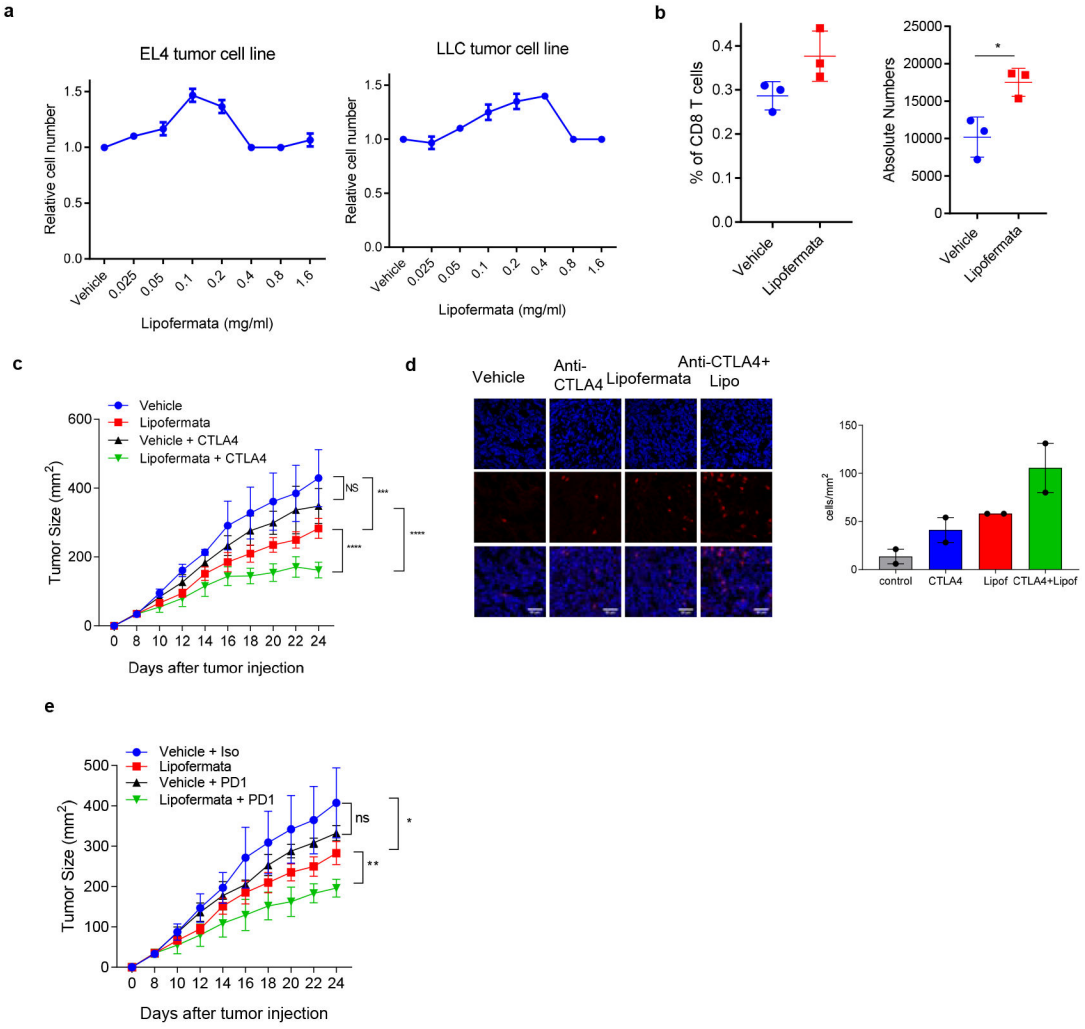

Extended data Figure 9. Effect of lipofermata treatment on tumor-bearing mice.

a. MTT assay after 3-day incubation of tumor cells with indicated concentration of lipofermata. **b**. Percentage and absolute number of tumor-associated antigen (E7-derived peptide) specific $CD8^+$ T cells in draining lymph nodes of mice bearing TC-1 tumor and treated with lipofermata (n=3). Means and SD are shown. P values were calculated in two-sided Student's *t*-test: *P<0.05; **c.** Growth of TC-1 tumors in mice treated with CTLA4 antibody and lipofermata (n=5). Mean and SD are shown. **d.** $CD8^+$ T cell infiltration of TC-1 tumors in mice treated with CTLA4 antibody and lipofermata. Typical staining of 2 different mice is shown. Scale bar = 50 μm. Bottom – the number of CD8+ T cells per mm2 (n=2). **e.** Growth of TC-1 in mice treated with PD1 antibody and lipofermata (n=5). Mean ± SD are shown. P values are calculated in two-way ANOVA test with correction for repeated measurements. *P<0.05; **P<0.01; ***P<0.001; ****P<0.0001.

Extended data Table 1.

Major phospholipid molecular species, containing deuterated arachidonic acid in WT and FATP2 KO PMN.

Phospholipid molecular species are represented as di-acyl and alkenyl/acyl species: PE(16:0/20:4) and PE(16:0p/20:4), respectively. These m/z values indicate ratios of mass to charge [M + Formate]- ions for PC and [M - H]- ions for the rest of phospholipids PE, PI, PS, PG, BMP, PA, respectively. Data are mean + SD; differences were detected by Student's t-test. N = 5.

PL Molecular species	m/z	ppm	pmol/mg protein		
			WT	FATP2 KO	*p value*
PE(16:0/20:4d11)	749.5718	3.3	32.17 + 4.58	21.92 + 3.98	*0.010*
PE(18:0/20:4d11)	777.6079	0.9	119.83 + 14.37	72.62 + 14.22	*0.002*
PE(16:0p/20:4d11)	733.5833	3.2	218.51 + 41.30	131.27 + 17.43	*0.006*
PE(18:0p/20:4d11)	761.6130	0.9	279.61 + 57.35	142.52 + 11.91	*0.002*
PC(16:0/20:4d11)	837.6300	2.0	233.07 + 33.78	140.29 + 24.39	*0.003*
PC18:0/20:4d11)	865.6615	2.2	307.33 + 35.30	145.28 + 20.37	*0.001*
PC18:1/20:4d11)	863.6464	2.9	115.63 + 12.99	62.45 + 10.64	*0.001*
PC(16:0p/20:4d11)	821.6321	-0.4	20.72 + 4.25	10.26 + 2.60	*0.004*
PC(18:0p/20:4d11)	849.6662	1.8	478.76 + 92.27	232.63 + 32.48	*0.002*
PI(18:0/20:4d11)	896.6181	0.3	472.19 + 65.28	323.03 + 37.99	*0.005*
PS(18:0/20:4d11)	821.5989	2.9	93.44 + 28.97	68.20 + 9.77	*0.143*
PG(18:0/20:4d11)	808.6046	1.6	1.44 + 0.25	0.80 + 0.12	*0.002*
BMP(18:0/20:4d11)	808.6046	1.6	0.04 + 0.02	0.02 + 0.04	*0.463*
PA(16:0/20:4d11)	706.5362	1.4	7.44 + 1.62	3.65 + 1.20	*0.006*
PA18:0/20:4d11)	734.5683	3.8	52.40 + 8.87	31.22 + 6.83	*0.006*
PA18:1/20:4d11)	732.5525	4.4	4.45 + 1.15	1.54 + 0.62	*0.003*

Supplementary Material

Refer to Web version on PubMed Central for supplementary material.

Acknowledgements

This work was supported by NIH grant CA R01CA165065 to D.I.G and V.E.K., NIH grant AI110485 to M.B., and by animal, genomics, and flow cytometry core facilities of Wistar Institute. We thank Dr. R. Schreiber (Washington University, St. Louis, MO) for providing us with F244 cells, Dr. L. Joannas and J. Henao-Meja from CRISPR/Cas9 Mouse Targeting Core of University of Pennsylvania for generating *slc27a2*$^{fl/fl}$ mice, Dr. Stremmel (University of Heidelberg, Germany) for providing *Slc27a4*$^{fl/fl}$ mice, Dr. D. Weiner (Wistar Institute) for providing tetramers.

References

1. Zhou J, Nefedova Y, Lei A & Gabrilovich D Neutrophils and PMN-MDSC: Their biological role and interaction with stromal cells. Semin Immunol 35, 19–28, doi:10.1016/j.smim.2017.12.004 (2018). [PubMed: 29254756]
2. Veglia F, Perego M & Gabrilovich D Myeloid-derived suppressor cells coming of age. Nat Immunol 19, 108–119, doi:10.1038/s41590-017-0022-x (2018). [PubMed: 29348500]
3. Gabrilovich DI, Ostrand-Rosenberg S & Bronte V Coordinated regulation of myeloid cells by tumours. Nat Rev Immunol 12, 253–268 (2012). [PubMed: 22437938]
4. Kumar V, Patel S, Tcyganov E & Gabrilovich DI The Nature of Myeloid-Derived Suppressor Cells in the Tumor Microenvironment. Trends Immunol 37, 208–220, doi:10.1016/j.it.2016.01.004 (2016). [PubMed: 26858199]
5. Moore KJ, Sheedy FJ & Fisher EA Macrophages in atherosclerosis: a dynamic balance. Nat Rev Immunol 13, 709–721, doi:10.1038/nri3520 (2013). [PubMed: 23995626]
6. O'Neill LA & Pearce EJ Immunometabolism governs dendritic cell and macrophage function. J Exp Med 213, 15–23, doi:10.1084/jem.20151570 (2016). [PubMed: 26694970]
7. Hubler MJ & Kennedy AJ Role of lipids in the metabolism and activation of immune cells. J Nutr Biochem 34, 1–7, doi:10.1016/j.jnutbio.2015.11.002 (2016). [PubMed: 27424223]
8. Veglia F et al. Lipid bodies containing oxidatively truncated lipids block antigen cross-presentation by dendritic cells in cancer. Nature communications 8, 2122, doi:10.1038/s41467-017-02186-9 (2017).
9. Ramakrishnan R et al. Oxidized lipids block antigen cross-presentation by dendritic cells in cancer. J Immunol 192, 2920–2931, doi:10.4049/jimmunol.1302801 (2014). [PubMed: 24554775]
10. Herber DL et al. Lipid accumulation and dendritic cell dysfunction in cancer. Nat Med 16, 880–886 (2010). [PubMed: 20622859]
11. Cubillos-Ruiz JR et al. ER Stress Sensor XBP1 Controls Anti-tumor Immunity by Disrupting Dendritic Cell Homeostasis. Cell 161, 1527–1538, doi:10.1016/j.cell.2015.05.025 (2015). [PubMed: 26073941]
12. Al-Khami AA et al. Exogenous lipid uptake induces metabolic and functional reprogramming of tumor-associated myeloid-derived suppressor cells. Oncoimmunology 6, e1344804, doi: 10.1080/2162402X.2017.1344804 (2017). [PubMed: 29123954]
13. den Brok MH, Raaijmakers TK, Collado-Camps E & Adema GJ Lipid Droplets as Immune Modulators in Myeloid Cells. Trends Immunol 39, 380–392, doi:10.1016/j.it.2018.01.012 (2018). [PubMed: 29478771]
14. Black PN & DiRusso CC Yeast acyl-CoA synthetases at the crossroads of fatty acid metabolism and regulation. Biochim Biophys Acta 1771, 286–298, doi:10.1016/j.bbalip.2006.05.003 (2007). [PubMed: 16798075]
15. Black PN, Ahowesso C, Montefusco D, Saini N & DiRusso CC Fatty Acid Transport Proteins: Targeting FATP2 as a Gatekeeper Involved in the Transport of Exogenous Fatty Acids. MedChemComm 7, 612–622, doi:10.1039/C6MD00043F (2016). [PubMed: 27446528]
16. Nicks KM et al. Three-dimensional structural analysis of the proximal femur in an age-stratified sample of women. Bone 55, 179–188, doi:10.1016/j.bone.2013.02.009 (2013). [PubMed: 23486182]
17. Youn JI, Collazo M, Shalova IN, Biswas SK & Gabrilovich DI Characterization of the nature of granulocytic myeloid-derived suppressor cells in tumor-bearing mice. J Leukoc Biol 91, 167–181, doi:10.1189/jlb.0311177 (2012). [PubMed: 21954284]
18. Rodriguez PC et al. Arginase I in myeloid suppressor cells is induced by COX-2 in lung carcinoma. J Exp Med 202, 931–939 (2005). [PubMed: 16186186]
19. Sinha P, Clements VK, Fulton AM & Ostrand-Rosenberg S Prostaglandin E2 promotes tumor progression by inducing myeloid-derived suppressor cells. Cancer Res 67, 4507–4513 (2007). [PubMed: 17483367]
20. Li Y et al. Myeloid-derived suppressor cells as a potential therapy for experimental autoimmune myasthenia gravis. J Immunol 193, 2127–2134, doi:10.4049/jimmunol.1400857 (2014). [PubMed: 25057008]

21. Mei Z, Korotkova O & Mao Y Products of Schell-model cross-spectral densities. Opt Lett 39, 6879–6882, doi:10.1364/OL.39.006879 (2014). [PubMed: 25503020]
22. He Y-M et al. Transitory presence of myeloid-derived suppressor cells in neonates is critical for control of inflammation Nat Med in press (2018).
23. Casbon AJ et al. Invasive breast cancer reprograms early myeloid differentiation in the bone marrow to generate immunosuppressive neutrophils. Proc Natl Acad Sci U S A 112, E566–575, doi:10.1073/pnas.1424927112 (2015). [PubMed: 25624500]
24. Condamine T et al. Lectin-type oxidized LDL receptor-1 distinguishes population of human polymorphonuclear myeloid-derived suppressor cells in cancer patients. Sci Immunol 1, doi: 10.1126/sciimmunol.aaf8943 (2016).
25. Ahowesso C et al. Chemical inhibition of fatty acid absorption and cellular uptake limits lipotoxic cell death. Biochem Pharmacol 98, 167–181, doi:10.1016/j.bcp.2015.09.004 (2015). [PubMed: 26394026]
26. Kumar V et al. Cancer-Associated Fibroblasts Neutralize the Anti-tumor Effect of CSF1 Receptor Blockade by Inducing PMN-MDSC Infiltration of Tumors. Cancer Cell 32, 654–668 e655, doi: 10.1016/j.ccell.2017.10.005 (2017). [PubMed: 29136508]
27. Zelenay S et al. Cyclooxygenase-Dependent Tumor Growth through Evasion of Immunity. Cell 162, 1257–1270, doi:10.1016/j.cell.2015.08.015 (2015). [PubMed: 26343581]
28. Fujita M et al. COX-2 blockade suppresses gliomagenesis by inhibiting myeloid-derived suppressor cells. Cancer Res 71, 2664–2674, doi:10.1158/0008-5472.CAN-10-3055 (2011). [PubMed: 21324923]
29. Veltman JD et al. COX-2 inhibition improves immunotherapy and is associated with decreased numbers of myeloid-derived suppressor cells in mesothelioma. Celecoxib influences MDSC function. BMC cancer 10, 464, doi:10.1186/1471-2407-10-464 (2010). [PubMed: 20804550]
30. He YM et al. Transitory presence of myeloid-derived suppressor cells in neonates is critical for control of inflammation. Nat Med 24, 224–231, doi:10.1038/nm.4467 (2018). [PubMed: 29334374]
31. Henao-Mejia J et al. Generation of Genetically Modified Mice Using the CRISPR-Cas9 Genome-Editing System. Cold Spring Harb Protoc 2016, pdb prot090704, doi:10.1101/pdb.prot090704 (2016).
32. Langmead B & Salzberg SL Fast gapped-read alignment with Bowtie 2. Nat Methods 9, 357–359, doi:10.1038/nmeth.1923 (2012). [PubMed: 22388286]
33. Li B & Dewey CN RSEM: accurate transcript quantification from RNA-Seq data with or without a reference genome. BMC bioinformatics 12, 323, doi:10.1186/1471-2105-12-323 (2011). [PubMed: 21816040]
34. Love MI, Huber W & Anders S Moderated estimation of fold change and dispersion for RNA-seq data with DESeq2. Genome biology 15, 550, doi:10.1186/s13059-014-0550-8 (2014). [PubMed: 25516281]
35. Chen HS et al. BET-Inhibitors Disrupt Rad21-Dependent Conformational Control of KSHV Latency. PLoS Pathog 13, e1006100, doi:10.1371/journal.ppat.1006100 (2017). [PubMed: 28107481]
36. Michelini Z et al. Development and use of SIV-based Integrase defective lentiviral vector for immunization. Vaccine 27, 4622–4629, doi:10.1016/j.vaccine.2009.05.070 (2009). [PubMed: 19523909]
37. Negri D et al. Immunization with an SIV-based IDLV Expressing HIV-1 Env 1086 Clade C Elicits Durable Humoral and Cellular Responses in Rhesus Macaques. Mol Ther, doi:10.1038/mt. 2016.123 (2016).

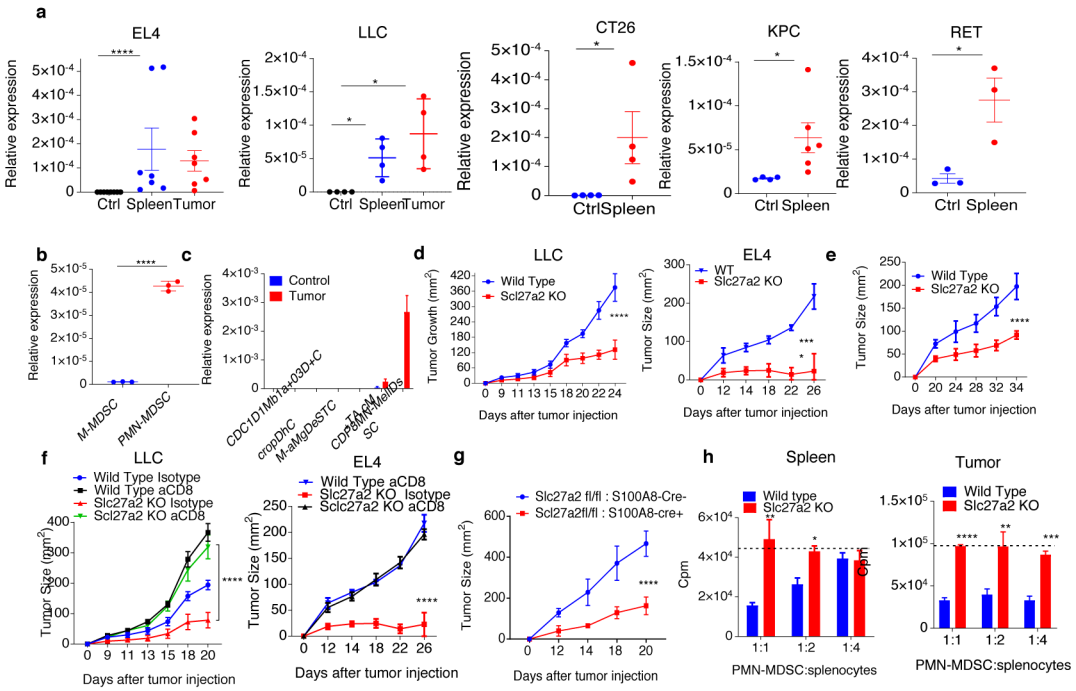

Figure 1. The effect of FATP2 deletion on tumor growth and PMN-MDSC function.

a. *Slc27a2* expression in control PMN and PMN-MDSC from TB mice. **b.** *Slc27a2* expression in M-MDSC and PMN-MDSC from spleen of TB mice. **c.** *Slc27a2* expression in indicated cells in EL4 TB mice. In **a-c** results of individual mice are shown. N=4–5. **d.** EL4 or LLC tumor growth in C57BL/6 mice (n=4–5). Representative of 2 experiments. **e.** EL4 tumor in mice reconstituted with WT or FATP2 KO BM cells. N=4–5. Representative of 2 experiments. **f.** EL4 or LLC tumors in WT and FATP2 KO mice depleted of $CD8^+$ T cells. Representative of 2 experiments (n=4–5). **g.** LLC tumors in mice with FATP2 KO targeted to PMN (S100A8-cre). N=4. **h.** Suppression of T-cell proliferation by PMN-MDSC isolated from WT or FATP2 KO TB mice. Four experiments with similar results were performed. Dashed line shows T cell proliferation without MDSC. In **d-g** p values were calculated in two-way ANOVA test. In all other panels p values were calculated using unpaired two-sided Student's t-test. In all panels *P<0.05; **P<0.01; ***P<0.001; ****P<0.0001 between control and test samples.

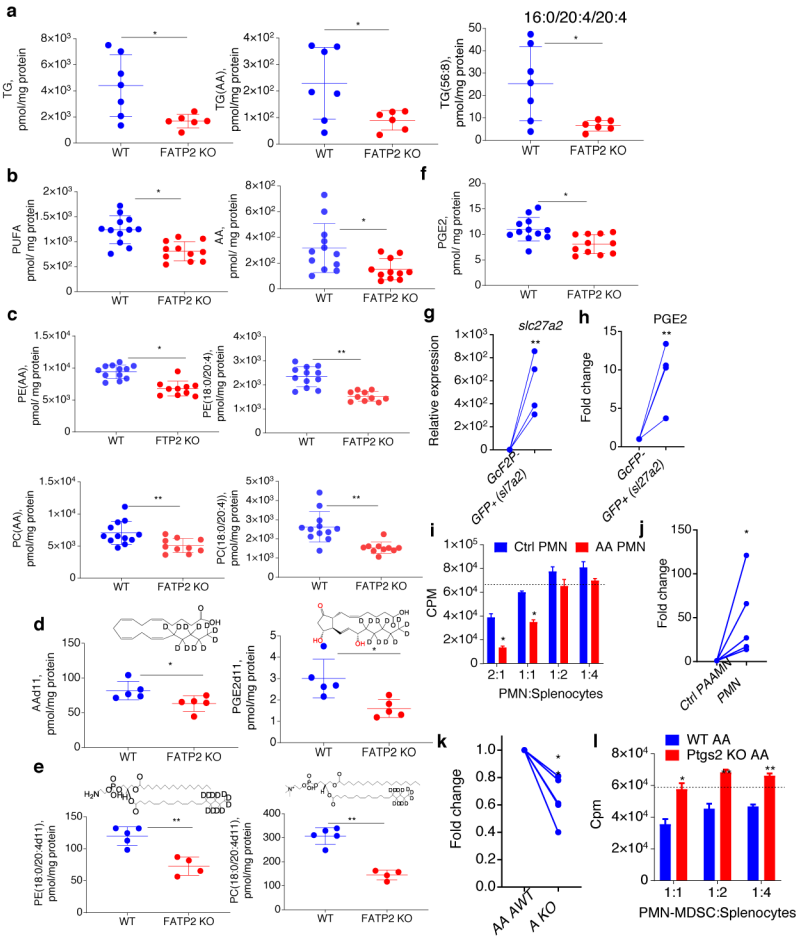

Figure 2. Mechanism of FATP2 mediated suppression by PMN-MDSC.

a. TG in PMN-MDSC from spleens of EL4 TB WT and FATP2 KO mice (n=7). **b.** FA in PMN-MDSC from spleen of TB WT (n=12) and FATP2 KO mice (n=11). **c.** Phospholipid species containing AA residues in PMN-MDSC from spleen of TB WT (n=12) and FATP2 KO mice (n=10). **d.** AAd11, and PGE2d11 in PMN-MDSC from spleen of TB WT and FATP2 KO mice (n=5). **e.** AAd11 labelled PE and PC in PMN-MDSC from WT (n=5) and FATP2 KO (n=4) TB mice. **f.** PGE2 (LS-MS) in PMN-MDSC from WT and FATP2 KO mice (n=6). **g.** Expression of *slc27a2* (qRT-PCR) in PMN generated from HPC transduced with lentivirus expressing FATP2 or GFP (n=4). **h.** PGE2 release from cells described in **g.** N=4. In **g,h -** fold increase over GFP^{-} cells after transduction. **i.** Suppressive activity (in triplicates) of PMN differentiated from HPC in the presence of AA. Representative of 3 experiments is shown. Dashed line shows T cell proliferation without MDSC. **j.** PGE2 production by PMN differentiated from HPC in the presence of AA (n=5). Fold changes over the control. **k.** PGE2 production by PMN differentiated from Ptgs2 KO HPC in the presence of AA. N=4. Fold changes over control. **l.** Suppressive activity (in triplicates) of PMN differentiated from Ptgs2 KO HPC in the presence of AA. Two independent experiments were performed. Dashed line shows T cell proliferation without MDSC. In all experiments Mean ± SD are shown and p values were calculated using unpaired two-sided

Student’s t-test. *P<0.05; **P<0.01; ***P<0.001; ****P<0.0001 between control and test samples.

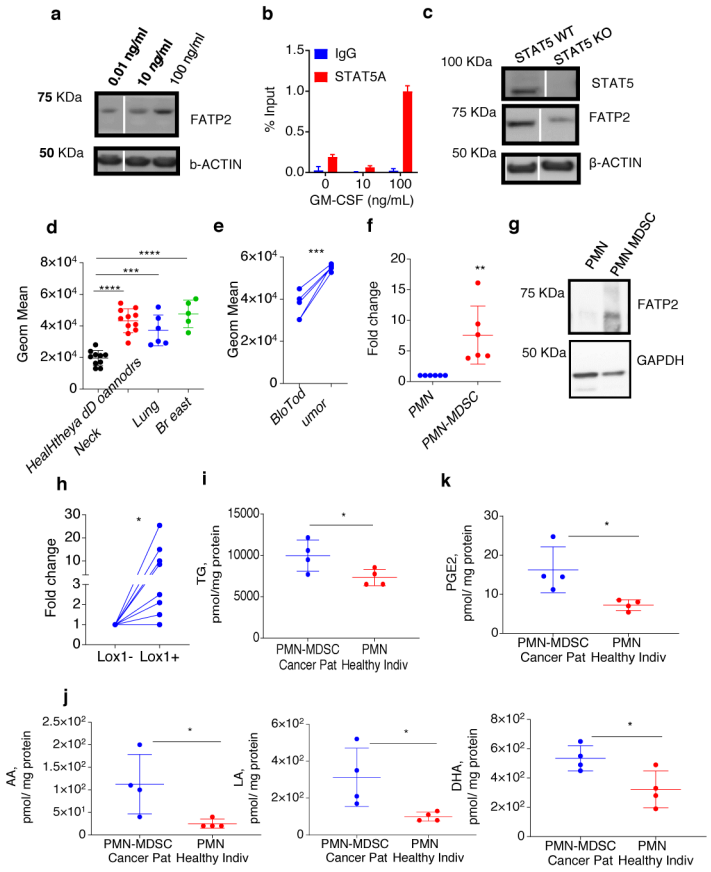

Figure 3. Regulation of FATP2 in PMN-MDSC.

a. FATP2 in PMN treated with GM-CSF. Representative of 3 experiments. For gel source data, see Supplementary Figure 1. **b.** ChIP assay with STAT5 antibody in PMN from BM treated with GM-CSF. Triplicate measurements of representative of 2 experiments are shown **c.** FATP2 in *stat5*$^{fl/fl}$:*s100a8*-cre PMN treated with GM-CSF. Representative of 3 experiments. **d.** Amount of lipid (BODIPY staining) in PMN-MDSC isolated from blood healthy individuals (n=9) or patients with head and neck cancer (n=11), non-small cell lung cancer (n=6), or breast cancer (n=5). **e.** Amount of lipid (BODIPY staining) in PMN-MDSC isolated from blood and tumor tissue of cancer patients with NSCLC (n=4). **f.** Expression of *SLC27A2* by RT-qPCR in PMN-MDSC isolated from blood of cancer patients and healthy donors. Fold change over control PMN (n=6). **g.** FATP2 in PMN-MDSC isolated from blood of cancer patients or healthy individuals. Representative of 3 experiments. **h.** *SLC27A2* expression by RT-qPCR in LOX1^{+} and LOX1^{-} PMN from blood of cancer patients. Fold change over LOX1^{-} PMN (n=8) **i.** LS/MS lipidomics of TG in PMN from healthy donors and PMN-MDSC from cancer patients. N=4. **j.** LS/MS lipidomics of free AA, LA, and DHA in PMN from healthy donors and PMN-MDSC from cancer patients (n=4). **k.** LS/MS lipidomics of PGE2 in PMN from healthy donors and PMN-MDSC from cancer patients (n=4). In all panels Mean ± SD are shown. Statistical analysis was performed using Two-Way ANOVA (**d**). In all other panels using unpaired two-sided Student's t-test: NS, not significant; *P<0.05; **P<0.01; ***P<0.001; ****P<0.0001.

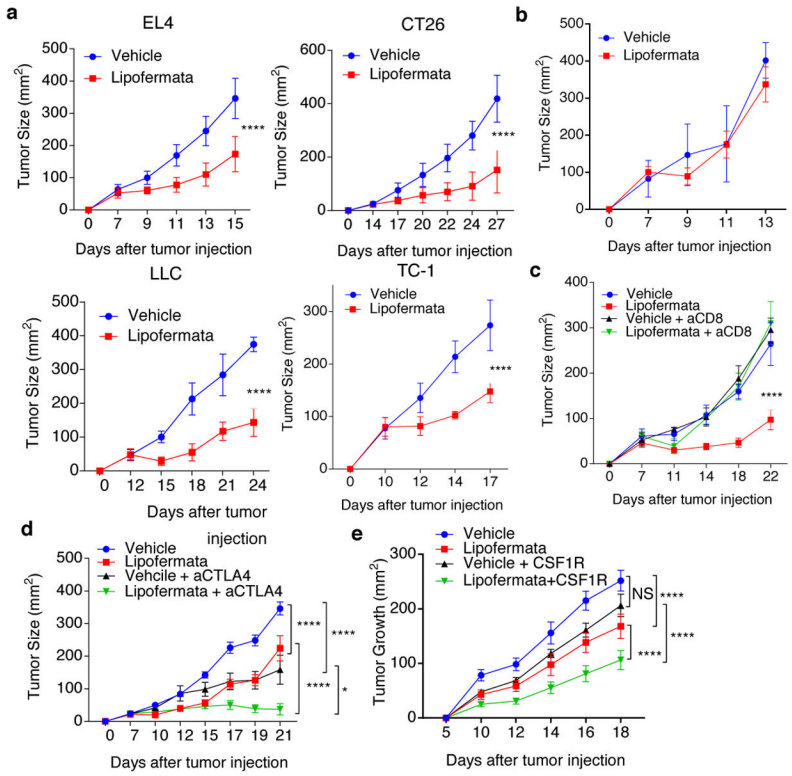

Figure 4. Therapeutic effect of targeting FATP2.

Treatments with lipofermata (2 mg/kg twice per day s.c.) started 8–10 days after tumors injections. CTLA4 antibody (200 μg/mouse i.p.) was administrated at day 7 and day 11 after tumor injection. CSF1R antibody (300 μg/mouse; every other day). **a.** Growth of indicated tumors in C57BL/6 mice treated with lipofermata. Representative of 2 independent experiments (n= 4–5 mice per group) are shown. **b.** Growth of LLC tumors in NOD-SCID mice treated with lipofermata (n=5). **c.** Growth of LLC tumor in mice depleted of CD8 T cells and treated with lipofermata (n=5). **d.** Growth of LLC tumor in mice treated with CTLA4 antibody and lipofermata (n=5). **e.** Growth of LLC tumor in mice treated with CSF1R inhibitor and lipofermata (n=5). In all experiments Mean ± SEM are shown and statistical analysis was performed in two-way ANOVA test with corrections for multiple comparison *P<0.05; **P<0.01; ***P<0.001; ****P<0.0001 differences from untreated cells and between treated groups.